Matrix Isolation and Transient Absorption Studies of (Bis(bis(pentafluoroethyl)phosphino)ethane)tetracarbonylchromium: Intermolecular Alkane Complexes and Intramolecular F-Coordination

Maurice Brookhart,*,† Wayne Chandler,† Robert J. Kessler,† Yumin Liu,† Norbert J. Pienta,† Catherine C. Santini,† Chris Hall,‡ Robin N. Perutz,*,‡ and John A. Timney§

Contribution from the Department of Chemistry, University of North Carolina, Chapel Hill, North Carolina 27599-3290, Department of Chemistry, University of York, York YO1 5DD, United Kingdom, and School of Education, University of Newcastle upon Tyne, Newcastle upon Tyne, NE1 7RU, United Kingdom. *Received August 22, 1991*

Abstract: Photolysis of (η^2-dfepe)$Cr(CO)_4$ [dfepe = $(C_2F_5)_2PCH_2CH_2P(C_2F_5)_2$] has been conducted in rigid matrices at 12 K (Ar, CH_4, N_2, CO) and 30 K (Xe) and in alkane and perfluoroalkane solutions. In Ar, CH_4, and Xe matrices a combination of IR and UV-vis spectroscopic data demonstrate photodissociation of the cis carbonyl ligand to generate *fac*-(dfepe)$Cr(CO)_3L$, where L is either the matrix host or an intramolecularly coordinated F atom donated by one of the pendant CF_3CF_2- groups of the dfepe ligand. Only traces of the mer isomer were observed. In nitrogen matrices there is evidence for formation of both *fac*- and *mer*-(dfepe)$Cr(CO)_3N_2$. Carbonyl stretching frequencies of the matrix-isolated photoproducts were measured and bonding force constants and ligand effect constants were calculated. In solution both the Cr-CO and Cr-P bonds are photolabile. Results of nanosecond and microsecond transient absorption spectroscopic experiments in hexane and cyclohexane solvents indicate formation of alkane complexes of the type (η^2-dfepe)$Cr(CO)_3$(alkane) and (η^1-dfepe)$Cr(CO)_4$(alkane), as well as formation of intramolecularly F-coordinated species $Cr(CO)_4$(η^1-dfepe) and $Cr(CO)_3$(η^2-dfepe). By use of transient absorption techniques, rates of reaction of these species in alkane solvents with and without added trapping ligands (CO, water, triethylsilane) have been measured. The F-coordinated species react with CO approximately 50 times faster than the alkane complexes. In experiments using (η^1-dfepe)$Cr(CO)_5$, similar results have been obtained which support the interpretation of the behavior of (η^2-dfepe)$Cr(CO)_4$. Products from ^{13}CO trapping of the transients generated in hexane show that all four possible isomers, *fac*- and *mer*-(η^2-dfepe)$Cr(CO)_3$*CO and *cis*- and *trans*-(η^1-dfepe)$Cr(CO)_4$*CO, are formed in significant quantities. Experiments carried out at a different ^{13}CO pressures show that ^{13}CO trapping of *cis*-(η^1-dfepe)$Cr(CO)_4$(L) is competitive with ring closure back to (η^2-dfepe)$Cr(CO)_4$.

Introduction

The irradiation of metal carbonyl complexes affords an efficient and general method for the generation and study of new complexes in which one or more carbonyls have been replaced by other ligands.[1] The mechanism and dynamics of the entire process have been elucidated for some of the best studied examples like $Cr(CO)_6$. Thus, the photochemistry and photophysics of $Cr(CO)_6$ have been investigated in the picosecond regime by UV-vis[2] and infrared transient absorption spectroscopy,[3] by time-resolved Raman techniques[4] and laser flash photolysis[5] and photoacoustic calorimetry[6] in the nanosecond/microsecond regime, as well as by matrix isolation techniques.[7] The previous studies at ultrafast times suggest that $Cr(CO)_6$ loses CO very rapidly, within 500 fs,[2b] and the resulting 16-electron complex ligates the solvent or matrix material within a few picoseconds.[2] Although the structure of the 16-electron intermediate and the details surrounding these early times are somewhat controversial,[2-4] the square-pyramidal complex $Cr(CO)_5(S)$ (where S = solvent) is most assuredly formed within tens of picoseconds. Much of the subsequent chemistry involves thermal reactions and can be observed on nanosecond and slower time scales.

A wide variety of transition-metal complexes are now known in which a C-H bond serves as a two-electron donor ligand for a highly electrophilic metal center and forms a three-center, two-electron M···H···C agostic bond.[8] To date only agostic species involving *intramolecular* C-H coordination have shown sufficient stability and lifetimes to allow isolation or characterization in solution by NMR spectroscopy. No stable intermolecular alkane complexes have been isolated.[8c] The $M(CO)_6$ (M = Cr, Mo, W) systems are of interest in this regard in that low-temperature photolyses in methane matrices show evidence for an $M(CO)_5(CH_4)$ complex,[7] and nanosecond and picosecond laser transient

† University of North Carolina.
‡ University of York.
§ University of Newcastle upon Tyne.

(1) (a) Poliakoff, M.; Weitz, E. *Adv. Organomet. Chem.* **1986**, *25*, 277-316. (b) Dobson, G. R. *Acc. Chem. Res.* **1976**, *9*, 300. (c) Wrighton, M. *Inorganic and Organometallic Photochemistry*; American Chemical Society: Washington, DC, 1978.

(2) (a) Simon, J. D.; Peters, K. S. *Chem. Phys. Lett.* **1983**, *98*, 53. Simon, J. D.; Xie, X. *J. Phys. Chem.* **1986**, *90*, 6751. Simon, J. D.; Xie, X. *J. Phys. Chem.* **1987**, *91*, 5538. Simon, J. D.; Xie, X. *J. Phys. Chem.* **1989**, *93*, 291. Simon, J. D.; Xie, X. *J. Am. Chem. Soc.* **1990**, *112*, 1130. (b) Joly, A. G.; Nelson, K. A. *J. Phys. Chem.* **1989**, *93*, 2876. Joly, A. G.; Nelson, K. A. *Chem. Phys.* **1991**, *152*, 69. (c) Lee, M.; Harris, C. B. *J. Am. Chem. Soc.* **1989**, *111*, 8913.

(3) (a) Wang, L.; Zhu, X.; Spears, K. G. *J. Am. Chem. Soc.* **1988**, *110*, 8695. (b) Wang, L.; Zhu, X.; Spears, K. G. *J. Phys. Chem.* **1989**, *93*, 2.

(4) Yu, S.-C.; Xu, X.; Lingle, R.; Hopkins, J. B. *J. Am. Chem. Soc.* **1990**, *112*, 3668.

(5) (a) Kelly, J. M.; Hermann, H.; Koerner von Gustorf, E. *J. Chem. Soc., Chem. Commun.* **1973**, 105. (b) Kelly, J. M.; Bent, D. V.; Hermann, H.; Schulte-Frohlinde, D.; Koerner von Gustorf, E. *J. Organomet. Chem.* **1974**, *69*, 259. (c) Bonneau, R.; Kelly, J. M. *J. Am. Chem. Soc.* **1980**, *102*, 1220. (d) Hermann, H.; Grevels, F. W.; Henne, A.; Schaffner, K. *J. Phys. Chem.* **1982**, *86*, 5151. (e) Kelly, J. M.; Long, C.; Bonneau, R. *J. Phys. Chem.* **1983**, *87*, 3344. (f) Church, S. P.; Grevels, F. W.; Hermann, H.; Schaffner, K. *Inorg. Chem.* **1985**, *24*, 418. (g) Schaffner, K.; Grevels, F. W. *J. Mol. Struct.* **1988**, *173*, 51. (h) Brown, C. E.; Ishikawa, Y.; Hackett, P. A.; Rayner, D. M. *J. Am. Chem. Soc.* **1990**, *112*, 2530.

(6) (a) Bernstein, M.; Simon, J. D.; Peters, K. S. *Chem. Phys. Lett.* **1983**, *100*, 241. (b) Simon, J. D.; Bernstein, M.; Peters, K. S. *Laser Chem.* **1983**, *3*, 215. (c) Yang, G. K.; Vaida, V.; Peters, K. S. *Polyhedron* **1988**, *7*, 1619. (d) Morse, J. M., Jr.; Parker, G. H.; Burkey, T. J. *Organometallics* **1989**, *8*, 2471. (e) Burkey, T. J. *Polyhedron* **1989**, *8*, 2681.

(7) (a) Perutz, R. N.; Turner, J. J. *Inorg. Chem.* **1975**, *14*, 262. (b) Perutz, R. N.; Turner, J. J. *J. Am. Chem. Soc.* **1975**, *97*, 4791. (c) Burdett, J. K.; Graham, M. A.; Perutz, R. N.; Poliakoff, M.; Rest, A. J.; Turner, J. J.; Turner, R. F. *J. Am. Chem. Soc.* **1975**, *97*, 4805. (d) Burdett, J. K.; Grzybowski, J. M.; Perutz, R. N.; Poliakoff, M.; Turner, J. J.; Turner, R. F. *Inorg. Chem.* **1978**, *17*, 147. (e) Burdett, J. K.; Downs, A. J.; Gaskill, G. P.; Graham, M. A.; Turner, J. J.; Turner, R. F. *Inorg. Chem.* **1978**, *17*, 523.

0002-7863/92/1514-3802$03.00/0

absorption experiments indicate formation of short-lived $(CO)_5M$(alkane) species in solution.[2-6] $W(CO)_5$(ethane) has also been detected in the gas phase.[5h] The rate of recombination of $Cr(CO)_5$ with CO is dramatically increased in perfluorocarbon solvents,[5c] which cannot stabilize the intermediate.

Clearly, one would like to be able to exploit the unique electronic properties of the unsaturated 16-electron species with respect to alkane binding and activation without the concomitant loss of kinetic stability realized in the prototype $M(CO)_6$ complexes. In an effort to identify systems to meet these criteria and with an eye toward the generation of stable alkane complexes, we have chosen to examine $[(C_2F_5)_2PCH_2CH_2P(C_2F_5)_2]Cr(CO)_4$, **1**.[9] This complex and the 16-electron species $[(C_2F_5)_2PCH_2CH_2P(C_2F_5)_2]Cr(CO)_3$ generated by loss of CO possess several unique properties: (1) The perfluoroalkylphosphine ligand is a very strong π-acceptor and should mimic CO electronically.[9,10] (2) The steric bulk of the chelating phosphine ligand should prevent, or greatly retard, the rate of dimerization reactions involving (dfepe)$Cr(CO)_3$ or (dfepe)$Cr(CO)_3$(S) (dfepe = $(C_2F_5)_2PCH_2CH_2P(C_2F_5)_2$). Furthermore, rates of associative substitution reactions of (dfepe)$Cr(CO)_3$(S) may also be retarded. (3) No intramolecular C–H coordination in (dfepe)$Cr(CO)_3$ can occur in competition with an intermolecular C–H agostic interaction. (4) The perfluoroalkyl substituents render **1** soluble in extremely weakly coordinating perfluoroalkane solvents which may be required for hydrocarbon complex observation.

This paper describes the photochemistry of **1** both in matrices at low temperatures and in alkane and perfluoroalkane solvents at 22 °C. The solution experiments were conducted under steady-state conditions and with laser flash photolysis on nanosecond and microsecond time scales. For comparison we have isolated $Cr(CO)_5(\eta^1$-dfepe), **2**, and studied its photochemistry. Data suggest that a methane complex is formed in the methane matrix studies and that short-lived alkane complexes can be formed in solution. In addition, the evidence also supports the formation of a species containing an intramolecular Cr ← F–CF_2– bond in both matrices and alkane solutions. A complete mechanism for the behavior of **1** upon photolysis in alkane solvents is presented, including relative and absolute rate constants, for the series of events that occur on time scales as short as nanoseconds and as long as seconds. The significance of these results for the design and synthesis of transition-metal complexes that bind hydrocarbons will be discussed.

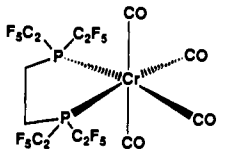

1

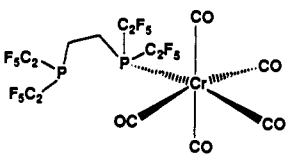

2

Our assignments of matrix IR spectra are supported by calculations employing ligand effect constant. This method, developed by Timney,[11] rationalizes CO stretching force constants in terms of a constant, k_d, for a first-row d^6 transition metal (Cr^0 in this instance) and two constants for each ligand (here CO and dfepe), ϵ^L_{cis} and ϵ^L_{trans}, describing their effect on the carbonyl in question. Thus the force constants for the axial and equatorial carbonyls of **1** would be given by eqs 1 and 2.

axial CO:

$$k_{CO} = k_d + \epsilon^{CO}{}_{trans} + 2\epsilon^{CO}{}_{cis} + 2\epsilon^{dfepe}{}_{cis} \quad (1)$$

equatorial CO:

$$k_{CO} = k_d + 3\epsilon^{CO}{}_{cis} + \epsilon^{dfepe}{}_{trans} + \epsilon^{dfepe}{}_{cis} \quad (2)$$

The ligand effect constants for dfepe may be derived from the IR spectrum of **1** and used in the calculation of CO force constants for other molecules containing dfepe. The ligand effect constants also provide a good measure of the π-acceptor capability of dfepe relative to other ligands.

Experimental Section

Precursor Syntheses. All reactions were conducted under a dry and oxygen-free argon or nitrogen atmosphere using Schlenk techniques with a double manifold vacuum line or a Vacuum Atmospheres drybox. Argon and nitrogen gases were purified by passage through a column of BASF catalyst (that had been activated by heating to 130 °C) followed by activated molecular sieves. Methylene chloride was distilled under an N_2 atmosphere from phosphorus pentaoxide prior to use. All alkane solvents (spectrophotometric grade), THF, and diethyl ether were dried by distillation from sodium benzophenone ketyl. Perfluoropentane was purified and dried by refluxing in the presence of calcium hydride for 3 days to a week and then passed through a 6 in. long column of activated alumina.[6d,e] To prepare ultradry samples, the above purified and dried alkanes and perfluoropentane solvents were stored over activated molecular sieves (24 h, 300 °C, in vacuo) in a drybox for at least 24 h. Solvents for column chromatography were degassed by purging with argon gas for 30 min. Deuterated solvents were used as received.

1,2-Bis(dichlorophosphino)ethane was prepared as previously described.[12a] Chloropentafluoroethane was purchased from PCR. Carbon monoxide was purchased from Linde and used as received. ^{13}CO was purchased from Aldrich.

^1H and ^{13}C NMR spectra were recorded on Varian XL400 and Bruker AC200 spectrometers in deuterated solvents. ^{31}P and ^{19}F NMR spectra were recorded on a Varian XL400 spectrometer. Chemical shifts are reported relative to residual protons in deuterated solvents ($CHDCl_2$, δ 5.32 ppm; C_6D_5H, δ 7.15 ppm; THF-d_7, δ 3.58 ppm). ^{31}P and ^{19}F were referenced externally to 85% H_3PO_4 (δ 0.00 ppm) and $C_6H_5CF_3$ (δ 0.00 ppm with upfield chemical shifts taken to be negative). Infrared spectroscopy was conducted on solutions in a sodium chloride cavity cell (0.2 mm path length) on a Mattson Polaris FTIR spectrometer using ICON software. Preparative photolyses were conducted by suspending solutions in Pyrex glassware 6–12 in. from a reflector flood lamp, GE HR100PFL44. Elemental analyses were performed by ORS, Inc., Whitesboro, NY.

Synthesis of $(C_2F_5)_2PCH_2CH_2P(C_2F_5)_2$. Bis(bis(pentafluoroethyl)-phosphino)ethane was prepared using a modification[30] of a literature procedure.[9]

Synthesis of $[(C_2F_5)_2PCH_2CH_2P(C_2F_5)_2]Cr(CO)_4$, 1. Complex **1** has been previously reported[9] and was prepared using the following alternative procedure. (THF)$Cr(CO)_5$ was generated by UV irradiation of 0.4 g (1.8 mmol) of $Cr(CO)_6$ in 150 mL of THF for 1.5 h. $(C_2F_5)_2PCH_2$-$CH_2P(C_2F_5)_2$ (1 g, 1.76 mmol) was added and the solution was stirred for 2 h at 70 °C. The solvent was removed under vacuum, and the residue was chromatographed with hexane on silica gel (R_f = 0.5), affording 1.01 g (80%) of the chromium complex **1**. This complex was recrystallized from pentane and sublimed (70–80 °C/0.25 mm) for further purification. IR (hexane): 2057 (m), 1995 (m), 1974 (vs) cm^{-1}. ^1H, ^{13}C, ^{19}F, and ^{31}P NMR data are similar to those previously reported.[9]

Synthesis of $[(C_2F_5)_2PCH_2CH_2P(C_2F_5)_2]Cr(CO)_5$, 2. (THF)$Cr(CO)_5$ (generated from 1 g (4.54 mmol) of $Cr(CO)_6$ in 150 mL of THF under UV irradiation for 8 h) and $(C_2F_5)_2PCH_2CH_2P(C_2F_5)_2$ (2.57 g, 4.54 mmol) were stirred together at room temperature. The progress of the reaction was monitored by IR spectroscopy. The reaction was judged to be complete by the disappearance of the (THF)$Cr(CO)_5$ bands at 1937 and 1894 cm^{-1} and the appearance of two new bands at 1977 and 2084 cm^{-1}. The solvent was removed on a vacuum line to yield a solid/oil mixture of $Cr(CO)_4$(dfepe) and $Cr(CO)_5$(dfepe). $Cr(CO)_6$ was also removed in this step and is collected in the vacuum trap at liquid nitrogen temperature. The resulting mixture was dissolved in a minimal amount

(8) (a) Brookhart, M.; Green, M. L. H.; Wong, L.-L. *Prog. Inorg. Chem.* **1988**, *36*, 1. (b) Crabtree, R. H.; Hamilton, D. G. *Adv. Organomet. Chem.* **1988**, *28*, 299. (c) Alkane complexes have been postulated as intermediates in thermolysis reactions of alkyl hydride complexes including $Cp_2W(H)(CH_3)$ (Bullock, R. M.; Headford, C. E. I.; Hennessy, K. M.; Kegley, S. E.; Norton, J. R. *J. Am. Chem. Soc.* **1989**, *111*, 3987.), $[Cp_2Re(H)CH_3]^+$ (Gould, G. L; Heinekey, D. M. *J. Am. Chem. Soc.* **1989**, *111*, 5503.) $Cp^*_2W(H)CH_3$ (Parkin, G.; Bercaw, J. E. *Organometallics* **1989**, *8* 1172.), and $Cp^*Rh(PMe_3)(H)$(alkyl) (Periana, R. A.; Bergman, R. G. *J. Am. Chem. Soc.* **1988**, *108*, 7332.).

(9) Complex **1** has been prepared previously: Ernst, M. R.; Roddick, D. M. *Inorg. Chem.* **1989**, *28*, 1624. For an alternative, higher yield procedure see ref 30.

(10) (a) Phillips, J. G.; Ball, R. G.; Cavell, R. G. *Inorg. Chem.* **1988**, *27*, 4038. (b) Burg, A. B.; Street, G. B. *J. Am. Chem. Soc.* **1963**, *85*, 3522. (c) Burg, A. B.; Street, G. B. *Inorg. Chem.* **1966**, *5*, 1532.

(11) Timney, J. A. *Inorg. Chem.* **1979**, *18*, 2502. Inquiries concerning computer programs for the analysis of ligand effect constants should be addressed to J.A.T. in Newcastle.

(12) (a) Henderson, R. A.; Hussain, W.; Leigh, G. J.; Normanton, F. B. *Inorg. Synth.* **1985**, *22*, 384. (b) Haddleton, D. M.; McCamley, A.; Perutz, R. N. *J. Am. Chem. Soc.* **1988**, *110*, 1810–13.

of hexane and cooled to −30 °C. The solution was filtered and $Cr(CO)_4$(dfepe) was collected as a solid. The solvent was removed from the mother liquor to yield $Cr(CO)_5$(dfepe) as an oil. Further purification of $Cr(CO)_5$(dfepe) was achieved by extracting the oil with 0.5 mL of CH_2Cl_2. The upper methylene chloride layer was removed via pipet. Trace amounts of solvent were removed under vacuum from the bottom layer containing **2** to give 0.9 g of $Cr(CO)_5$(dfepe) as a colorless oil (26% yield based on $Cr(CO)_6$). Anal. Calcd for $C_{15}H_4CrP_2F_{20}O_5$ [found (calcd)]: C, 23.71 (23.77); H, 0.58 (0.53). IR (CD_2Cl_2): 1976 (s), 2015 (w), 2084 (w) cm^{-1}. ^1H NMR (CD_2Cl_2, 400 MHz, 21 °C): δ 2.7 (m, CH_2, 2 H), 2.5 (m, CH_2, 2 H). ^{13}C NMR (CD_2Cl_2, 100 MHz, 21 °C): δ 216.9 (m, J_{PC} = 2 Hz, CO_{trans}), 213.3 (d, J_{PC} = 11.9 Hz, CO_{cis}), 120 (m, CF_3CF_2), 23.1 (dd, CH_2, J_{PC} = 12 Hz, J_{PC} = 30 Hz), 13.34 (d, CH_2, J_{PC} = 18 Hz). ^{31}P NMR (CD_2Cl_2, 161 MHz, 21 °C): δ 110.1 (m, Cr–P), 8.6 (m, free P).

Matrix Isolation Experiments. Matrix isolation experiments were performed with an apparatus which has previously been described in detail.[12b] In brief, the cold window was cooled by an Air Products CS202 cryogenic refrigerator mounted in a vacuum shroud pumped to 10^{-6} Torr before cooling. The window temperature was controlled by an Oxford Instruments temperature controller. Central and outer windows of barium fluoride were employed in order to obtain transparency over the full UV–vis range and the IR range above 1000 cm^{-1}. The entire apparatus is mounted on a trolley and may be moved reproducibly between spectrometers, so that IR and UV–vis spectra may be measured on the same samples. Fourier transform IR (FTIR) spectra were measured on a Mattson Sirius spectrometer at 1 cm^{-1} resolution with two-times zero-filling. UV–vis spectra were recorded on a Perkin-Elmer Lambda 7G spectrometer at 1 nm resolution. The matrices were photolyzed through a silica window with a focused Philips HPK 125-W medium-pressure mercury arc equipped with a water filter and appropriate cutoff or interference filters.

Complex **1**, prepared as described above, was purified by sublimation at 303 K and 10^{-3} Torr to give a white solid. Matrices were prepared by continuous deposition with the sample of **1** maintained at 293 K in a glass side arm, and the cold window held at 30 K for xenon, 25 or 20 K for CH_4, and 20 K for other matrix gases. The rate of deposition was 1.6 mmol h^{-1} for xenon and methane, and 2 mmol h^{-1} for the other gases; deposition times were typically 1–3 h. Subsequent photolysis and spectroscopic measurements were made at 30 K for Xe matrices and 12 K for the remaining matrices.

Steady Irradiation Experiments. Solutions of ca. 2–4 mg of **1** were prepared in a cuvette containing 2.5 mL of wet hexane (used as obtained) or in 2.5 mL of either CO-saturated hexane or hexane to which Et_3SiH (60–600 mM) had been added. The cuvettes were irradiated for a few minutes 4–6 in. from an HR100PFL44 sunlamp. The resulting solutions were analyzed by UV–vis spectroscopy. New peaks were observed in the case of wet solvent or added silane but not with CO saturated dry hexane. The new peaks in the visible spectrum grew with additional irradiation, and the solutions became yellow when irradiated for long times (30–60 min). The longest wavelength maximum of the starting material could be observed to diminish as new peaks grew in.

Photolysis Reactions of 1 under ^{13}CO. A quartz Schlenk tube was charged with 40 mg (0.05 mmol) of **1** and 40 mL of cyclohexane, subjected to three freeze–pump–thaw cycles, and finally filled with a pressure of ^{13}CO (99% labeled) determined by a mercury manometer on the vacuum/inert atmosphere line. The room-temperature solution was photolyzed with the sunlamp for 2 min. The solvent from an aliquot of the clear, colorless solution was removed in vacuo. The resulting white solid was dissolved in CD_2Cl_2, and the sample was analyzed by ^{13}C NMR spectroscopy. The percentage of ^{13}CO incorporation was calculated based on unlabeled **1**. In all cases incorporation of ^{13}CO was kept below 5% to minimize effects due to secondary photolysis of mono-^{13}C-labeled complex. Relative ratios of the variously labeled complexes **1** and **2** produced by photolysis at 115 and 295 mm of ^{13}CO were determined. ^{13}CO peak assignments were made on the following basis. In complex **1** the axial ^{13}CO is cis to both ^{31}P nuclei and appears as a simple triplet $^2J_{cis\text{-}PC}$ = 10.3 Hz at 215.3 ppm. The equatorial ^{13}CO at 220.6 ppm appears as a broadened doublet $^2J_{cis\text{-}PC}$ = 12.7 Hz indicating that in these perfluoroalkyl phosphine systems $^2J_{cis\text{-}PC}$ (ca. 10–12 Hz) > $^2J_{trans\text{-}PC}$ (< 2 Hz). In complex **2** the cis ^{13}CO (213.3 ppm, d, $^2J_{cis\text{-}PC}$ = 11.9 Hz) and trans ^{13}CO (216.9 ppm, small unresolved couplings) were assigned on the basis of their relative intensities in the unlabeled complex and further supported on the basis of the expected couplings $^2J_{cis\text{-}PC} > {}^2J_{trans\text{-}PC}$.

Nanosecond Transient Absorption Experiments. Nanosecond laser transient absorption data were collected with an apparatus that has been described previously.[13] Samples in this study were irradiated with the Nd:YAG third harmonic at 355 nm either parallel or perpendicular to the probe beam. The probe beam is a pulsed 250-W xenon arc lamp (Applied Photophysics). Typically, an entire spectrum was collected at 10 or 20 nm increments, and the rate data are the averages from such a set of 10–18 wavelengths for each solution. Individual decays at a single wavelength are an average of 10 shots, and each contain at least 500 points. Nonlinear least-squares regression was adapted from a public domain routine (D. Whitman, Cornell University) to DOS-based 386 microcomputers by FK Enterprises (Chapel Hill).

Samples were prepared in the indicated solvent with 2–20 mM precursor (OD of 0.5–1 at 355 nm) and degassed in a quartz apparatus that allowed freeze–pump–thaw cycles. The solutions were prepared in a glovebox and transferred into glassware fabricated in-house (a round-bottom flask attached to the 1 × 1 cm cell and the vacuum line joint by glass tubes). After being subjected to three cycles of freeze–pump–thaw degassing, the solution was sealed in the apparatus with a glass-blowing torch or first charged with 1 atm of CO and then sealed with a Teflon high-vacuum seal (that also served as the connection to the vacuum line). These samples were kept cold and dark until just prior to use. Ultradry samples were made from solutions that were transferred into such glassware that had been previously charged with 1–5 g of activated 3A molecular sieves.

Microsecond Transient Absorption Experiments. Experiments on the microsecond time scale were conducted using the same apparatus as described above with one exception. The probe beam was not pulsed but was used at a higher initial intensity in a continuous mode. The probe beam was adjusted to the desired intensity and illumination of the sample was controlled by an electronic shutter placed between the sample and the lamp, synchronized to the photolyzing laser pulse using home-built electronic circuitry.

Results

Matrix Isolation. The photolysis of $Cr(CO)_4$(dfepe), **1**, was investigated by UV–vis and IR spectroscopy in argon, xenon, methane, nitrogen-doped argon, and carbon monoxide matrices. The IR and UV–vis bands of the starting material and the photoproducts in each of the media are listed in Table I. Complex **1** exhibits three prominent bands in the CO-stretching region (Figure 1a); the band at lowest frequency is much more intense and somewhat broader than the others and probably arises from the overlap of two fundamentals. Weaker bands are detected from ^{13}CO-substituted **1**, present in natural abundance. The UV–vis spectrum of **1** in solid argon shows a band at 226 nm with a shoulder at 290 nm; these maxima shift less than 4 nm in Xe and CH_4 matrices.

Photolysis (λ > 285 nm) in argon, methane, or xenon matrices causes the depletion of the bands of **1**, the release of CO, the formation of a new product with three ν(CO) bands (ca. 2015, 1960, and 1920 cm^{-1}), and a prominent visible absorption maximum. The ν(CO) bands are shifted on average 45 cm^{-1} to low frequency of those of **1**. In argon matrices, 1 min photolysis causes 17% loss of **1**, increasing to 59% after 10 min, and 80% after 30 min. There are two other very weak product bands at ca. 2040 and 1940 cm^{-1}, which are already detectable after the 10 min of photolysis. After the initial 10-min photolysis with λ > 285 nm, the bands of the major product hardly increase, whereas those of **1** continue to decrease, indicating the formation of secondary products. On subsequent irradiation into the visible absorption band (λ > 460 nm, 720 min), both the UV–vis and the IR bands of the products decrease and those of the starting material recover to approximately half of their original intensity. The IR and visible product bands observed in the early stages of broad-band photolysis grow and decrease together, suggesting that they belong to a single species. Only with more selective photolysis (see below) is this shown to be incorrect.

When analogous experiments are performed in xenon or methane matrices, a similar pattern of behavior is observed, but with two notable differences: (i) complex **1** proves more photosensitive in methane than in argon with 58% of **1** converted to products after only 1 min of photolysis; (ii) the visible absorption band of the product shifts dramatically with matrix host moving from 554 nm in argon to 502 nm in both xenon and methane. The IR spectra observed in methane matrices are illustrated in Figure 1, which shows the effect of short-wavelength (Figure 1b) followed by long-wavelength photolysis (Figure 1d). The regeneration of

(13) Boyde, S.; Strouse, F. G.; Jones, W. E.; Meyer, T. J. *J. Am. Chem. Soc.* **1989**, *111*, 7448–54.

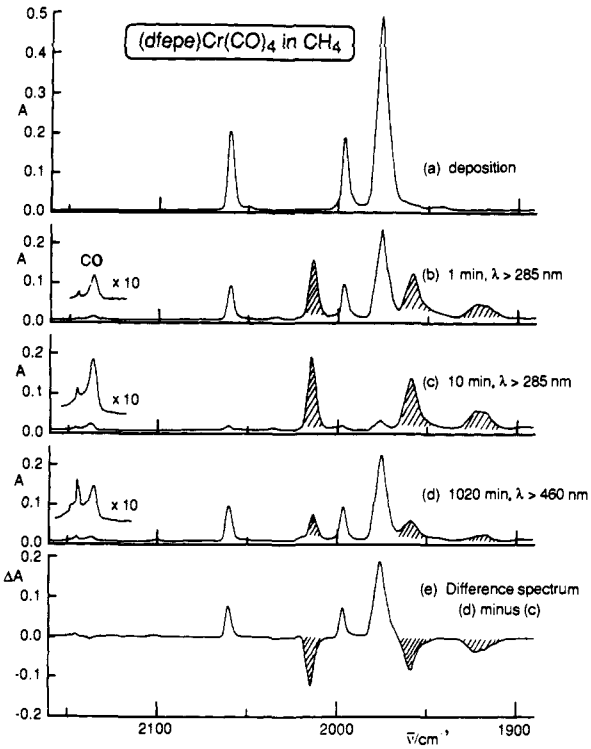

Figure 1. (a) IR spectrum in the CO stretching region of **1** in a methane matrix at 12 K (1 h deposition; sample temperature, 293 K; matrix temperature, 20 K; 1.6 mmol CH_4 deposited). (b) Spectrum after 1 min of mercury arc photolysis ($\lambda > 285$ nm) showing depletion of **1**, release of CO, and growth of *fac*-Cr(CO)$_3$(dfepe) (shaded). (c) Spectrum after a total of 10 min of photolysis ($\lambda > 285$ nm). (d) Spectrum after a further 1020 min of photolysis ($\lambda > 460$ nm) designed to irradiate into visible absorption band of the product. (e) Difference spectrum calculated as spectrum d minus spectrum c showing regeneration of **1** and loss of product.

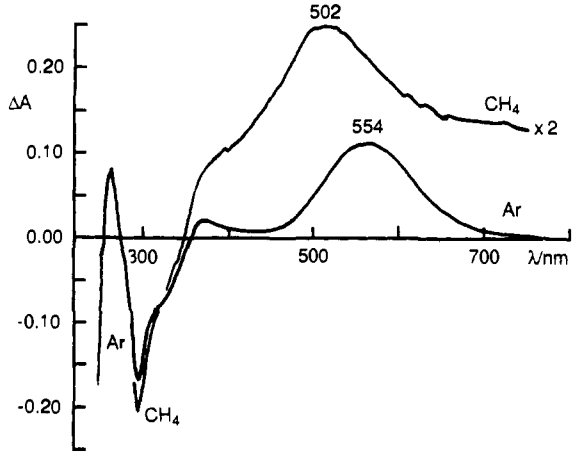

Figure 2. UV–vis spectra obtained following photolysis ($\lambda > 285$ nm) of **1** in argon or methane matrices at 12 K. The spectra are calculated as differences relative to the deposition spectrum, so the negative peaks correspond to **1**. Notice that the maxima of **1** are independent of the matrix, whereas those of the photoproduct, *fac*-Cr(CO)$_3$(dfepe) (shown positive), shift substantially with matrix.

1 can be seen as a difference spectrum in Figure 1e. The sensitivity of the visible bands of the product to the matrix host is shown in Figure 2.

Next we investigated the effect of more selective irradiation into the short- and long-wavelength tails of the visible band of the photoproduct in all three matrices. The results will be described in detail for methane, but the same pattern of behavior is observed for argon and xenon matrices. On photolysis with $\lambda = 434$ nm (8 h), the three IR bands of the major product and the weak band at ca. 2040 cm^{-1} each split into two components.

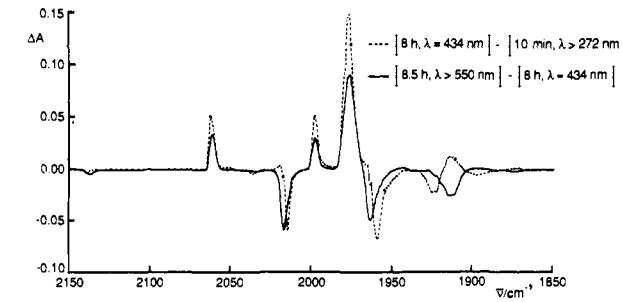

Figure 3. IR difference spectra in the ν(CO) region showing the effect of selective photolysis on **1** in a methane matrix. Initial photolysis for 20 min with $\lambda > 272$ nm (a) was followed by 8 h photolysis with $\lambda = 434$ nm (b) and then 8.5 h photolysis with $\lambda > 550$ nm (c): broken line, b–a; full line, c–b.

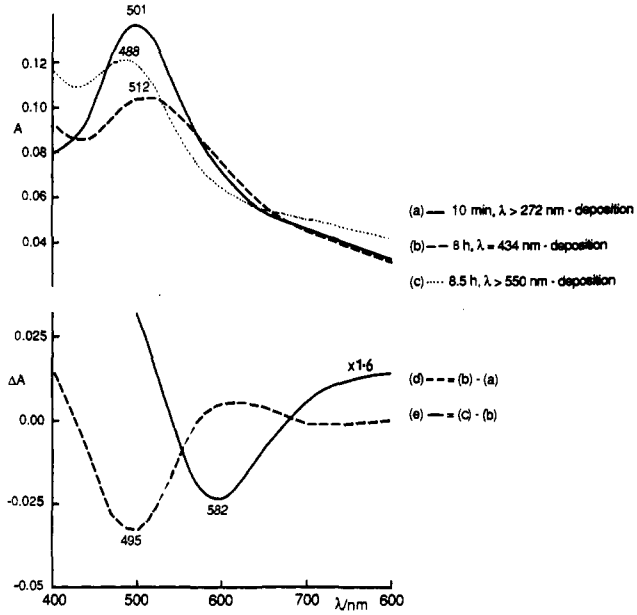

Figure 4. UV–vis spectra from the same experiment as illustrated in Figure 3. Photolysis stages a–c are indicated in the legend of Figure 3: above, spectra a, b, and c recorded relative to the deposition spectrum; below, (d) b – a, broken line; (e) c – b, full line.

One component (A) decreases substantially with concomitant growth of **1**, along with a slight increase in the other component (B) (see difference spectrum, Figure 3, broken line). This period of photolysis causes the visible maximum to shift from 501 to 512 nm (Figure 4a,b). A UV–visible difference spectrum shows a depletion peak at 495 nm (Figure 4d). After a final period of photolysis into the long-wavelength tail ($\lambda > 550$ nm, 8.5 h), component B of the IR product bands decreases substantially, leaving component A unaffected. Again the major product was **1**, and a decrease in the liberated CO could be detected (Figure 3, full line). The UV–visible maximum shifted to 488 nm (Figure 4c), and the difference spectrum relative to the previous stage of photolysis shows a depletion peak at 582 nm (Figure 4e).

These experiments demonstrate that two photoproducts are formed with very similar IR frequencies but dramatically different UV–vis spectra. The visible band maxima of component A, estimated from the difference spectra, are located at 545 nm (Ar), 495 nm (CH_4), and 490 nm (Xe), an overall shift from Ar to Xe of 2060 cm^{-1}. The maxima of component B shift far less: 590 nm (Ar), 582 nm (CH_4), and 578 nm (Xe), an overall shift of 350 cm^{-1}. It is evident from the UV–vis spectra that A and B differ not simply in conformation or trapping site, but more fundamentally.

The loss of CO on UV photolysis, the generation of product bands to low frequency of the starting material, and the recovery of starting material on long-wavelength photolysis are all features characteristic of the generation of a coordinatively unsaturated

Table I. IR (ν/cm^{-1}) and UV–vis (λ/nm) Bands of **1** and Its Photoproducts in Matrices at 12 K

		matrix Ar	CH_4	Xe	CO	Ar/5% N_2
$Cr(CO)_4$(dfepe)	IR	2062	2062	2060	2060	2061
		2001	1998	1996	1997	1999
		1980	1976	1976	1975	1977
fac-S···$Cr(CO)_3$(dfepe) (**4-S-*fac***)	IR	2020	2014	2013	2016[a]	2017[a]
		1965	1959	1956.5	1961[a]	1961[a]
		1922	1924	1924	1921[a]	1919[a]
	UV	545	495	490	458	554[a]
fac-F···$Cr(CO)_3$(dfepe) (**4-F-*fac***)	IR	2019	2017	2016		
		1964	1963	1962		
		1925	1914	1915		
	UV	590	582	578	574	
mer-S···$Cr(CO)_3$(dfepe) (**4-S-*mer***)	IR		2036	2034		
			1953 sh	1949 sh		
mer-F···$Cr(CO)_3$(dfepe) (**4-F-*mer***)	IR		2038	2036		
fac-$(N_2)Cr(CO)_3$(dfepe)	IR					2226 ν(NN)
						2022 ν(CO)
						1949 sh ν(CO)
	UV					363
mer-$(N_2)Cr(CO)_3$(dfepe)	IR					2212 ν(NN)
						2041 ν(CO)
	UV					363
secondary photoproducts			1897[b]		2102 (2)	2204 ν(NN)[c]
					2097 (2)	2170 ν(NN)[c]
					2022 (2)	
					1985 (3)	
					1965[d]	
					1933[d]	

[a] Not separated from **4-F-*fac*** by selective photolysis. [b] $Cr(CO)_2$(dfepe). [c] $(N_2)_2Cr(CO)_2$(dfepe). [d] CO···$Cr(CO)_5$.

metal carbonyl. Such behavior has now been observed for a wide variety of matrix-isolated metal carbonyls.[14] The major product may, therefore, be assigned to $Cr(CO)_3$(dfepe). The additional feature of a visible absorption band sensitive to the matrix material has been shown to be characteristic of d^6 square-pyramidal fragments such as (S)$M(CO)_5$ (M = Cr, Mo, W; S = matrix) and (S)$Mn(CO)_4H$ which are specifically solvated by the matrix.[7b,15]

The loss of CO from **1** could lead to two such species, either *fac*-$Cr(CO)_3$(dfepe) or the mer isomer. However, components A and B both have three ν(CO) bands with very similar frequencies, which decrease in intensity from high frequency to low frequency. These observations exclude the possibility that A and B represent the pair of isomers, fac and mer.[16,17] We also examined the possibility that one of the components is $Cr(CO)_4$-(η^1-dfepe) with a dangling phosphine ligand. This argument is discounted, since the amount of "free" CO is reduced at each stage of selective photolysis, whereas $Cr(CO)_4$(η^1-dfepe) should re-form **1** without reducing the CO. Moreover, predictions of the frequencies of $Cr(CO)_4$(η^1-dfepe) and $Cr(CO)_3$(dfepe) based on ligand effect constants for dfepe (see Discussion) exclude the possibility that either A or B is $Cr(CO)_4$(η^1-dfepe). On the other hand, these calculations support the assignment of *both* components A and B as *fac*-$Cr(CO)_3$(dfepe). The clue to solving this enigma comes from the UV–vis spectra which show that component A is specifically solvated by the matrix with band maxima very close to those of (S)$Cr(CO)_5$, while component B has UV–vis spectra almost independent of the matrix. The behavior of the UV–vis spectra can be understood if component B has a C_2F_5 group from dfepe coordinating weakly in the sixth position. In keeping with this hypothesis, the UV–vis maximum of B lies close to that of $(CF_4)Cr(CO)_5$ which has a similar sixth ligand.[7b] This assignment immediately explains the similarity of the IR spectra of components A and B. Thus, A is assigned as *fac*-(S)Cr-$(CO)_3$(dfepe) and B as the species with a fluorine in the sixth position represented as *fac*-[$(C_2F_5)_2PCH_2CH_2P(C_2F_5)CF_2CF_2$]-F→$Cr(CO)_3$ (**4-S-*fac*** and **4-F-*fac***, respectively). The very weak bands in the IR at ca. 2040 and 1950 cm^{-1} are consistent with assignments to the corresponding mer isomers, each band having a contribution from **4-S-*mer*** and **4-F-*mer*** (Table I).

Photolysis of **1** in solid CO causes relatively slow conversion to a tricarbonyl product with bands close to those observed in other matrices (13% conversion after 5 min, 22% after 20 min, $\lambda > 276$ nm). The UV–vis spectrum shows weak product bands at 574 and 458 nm. Such behavior can be interpreted if **1** is converted to **4-F-*fac*** with a band at 574 nm and to the "isocarbonyl" product *fac*-CO···($Cr(CO)_3$(dfepe) (λ_{max} 458 nm), in which one CO binds weakly through oxygen or in a dihapto mode (chromium pentacarbonyl behaves analogously).[7a,c] In this matrix, the solvated species is shifted to such short wavelength that it exhibits a separate peak from **4-F-*fac***. On prolonged photolysis a product band is also observed at 1985 cm^{-1}. Subsequent irradiation with the unfiltered arc ($\lambda > 200$ nm, 120 min) increases the loss of **1** to 98% and the 1985-cm^{-1} band becomes the most intense in the spectrum. Weak product bands are also observed at 2101, 2097, 2022, 1965, and 1933 cm^{-1}. The major product band at 1985 cm^{-1} coincides with that for $Cr(CO)_6$ in solid CO,[20] while the bands at 1965 and 1933 cm^{-1} correspond to CO···$Cr(CO)_5$.[7a] The bands at 2101, 2097, and 2022 cm^{-1} together with a contribution to the 1985-cm^{-1} band probably derive from $Cr(CO)_5$(η^1-dfepe), **2**.

When complex **1** is photolyzed in an argon matrix doped with 5% N_2, IR and visible bands are observed in almost identical positions to those for pure argon matrices; they are assigned to the $Cr(CO)_3$(dfepe) species **4-Ar-*fac*** and **4-F-*fac***. In addition, an intense UV band is formed at 363 nm, and further IR bands are detected in the carbonyl region and in the N–N stretching region between 2160 and 2240 cm^{-1}. After 1 min of photolysis ($\lambda > 285$ nm), two ν(NN) bands are detected at 2226 and 2212 cm^{-1}, but on further photolysis at the same wavelength, a third band is formed at 2204 cm^{-1} (Figure 5a). Photolysis for a total

(14) Hitam, R. B.; Mahmoud, K. A.; Rest, A. J. *Coord. Chem. Rev.* **1984**, *55*, 1.

(15) Church, S. P.; Poliakoff, M.; Timney, J. A.; Turner, J. J. *Inorg. Chem.* **1983**, *22*, 3259.

(16) Both fac and mer complexes are expected to show three IR-active CO-stretching modes. The highest frequency mode of the mer complex should be the symmetric stretching mode of the trans-oriented pair of carbonyl groups and is expected to be very weak. In contrast, all the bands of the fac complex should be reasonably intense, since the carbonyl groups are mutually orthogonal. A good example of these intensity patterns can be seen for (norbornadiene)$Mo(CO)_3(N_2)$. The three ν(CO) modes of the fac isomer are approximately equally intense, whereas the high-frequency mode of the mer isomer is approximately one-ninth of the intensity of the pair of overlapping low-frequency modes.[17]

(17) Jackson, S. A.; Hodges, P. M.; Poliakoff, M.; Turner, J. J.; Grevels, F.-W. *J. Am. Chem. Soc.* **1990**, *112*, 1221.

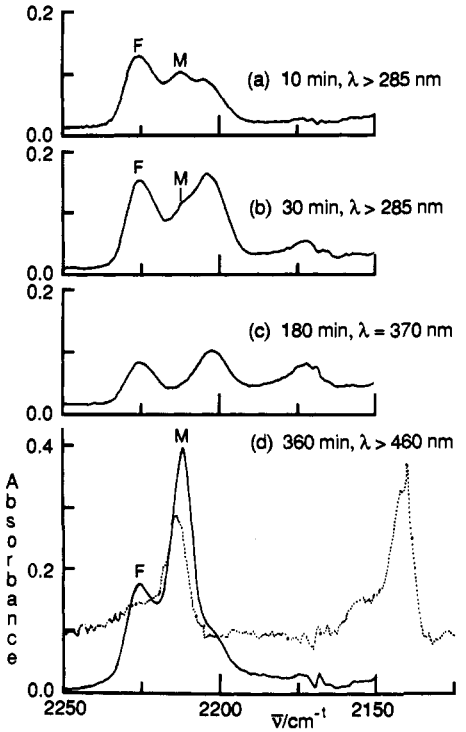

Figure 5. (a) IR spectrum in the N–N stretching region observed following 10 min photolysis of **1** in a 5% N_2/Ar matrix at 12 K (2.5 h deposition, sample at 293 K, window at 20 K, 4.9 mmol of gas deposited); (b) spectrum after a total of 30 min photolysis ($\lambda > 285$ nm); (c) spectrum after 180 min photolysis with $\lambda = 370$ nm which is selective for the dinitrogen products; (d) full line, spectrum after 360 min photolysis with $\lambda > 460$ nm which selects (Ar)Cr(CO)$_3$(dfepe): F = *fac*-(N_2)Cr(CO)$_3$(dfepe); M = *mer*-(N_2)Cr(CO)$_3$(dfepe): dotted line, spectrum at the corresponding stage of an experiment with **1** in $^{14}N_2/^{15}N_2$/Ar (2.5:2.5:95). The remaining bands illustrated are probably due to (N_2)$_2$Cr(CO)$_2$(dfepe). These spectra correspond exactly to the UV–vis spectra in Figure 6.

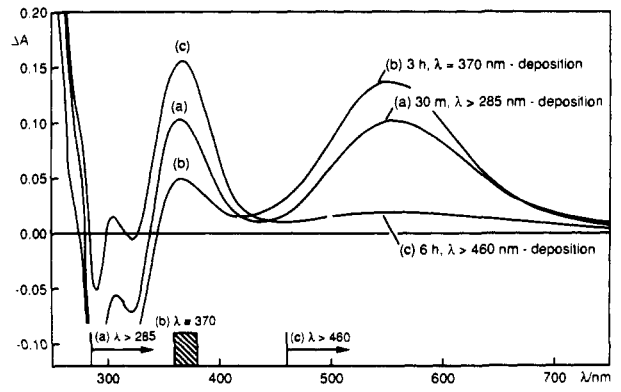

Figure 6. (a) UV–vis spectrum recorded following 30 min of photolysis ($\lambda > 285$ nm) of **1** in a 5% N_2/Ar matrix at 12 K. (b) Spectrum after 3 h of photolysis with $\lambda = 370$ nm, which is selective for the dinitrogen products. (c) Spectrum after 720 min of photolysis with $\lambda > 460$ nm, which selects **4-Ar-*fac*** and **4-F-*fac***. The band at 363 nm is due to *fac*- and *mer*-(N_2)Cr(CO)$_3$(dfepe), that at 554 nm due to **4-Ar-*fac*** and **4-F-*fac***. The wavelengths of photolysis are illustrated schematically. These spectra correspond exactly to the IR spectra in Figure 5b–d.

of 30 min increases all the dinitrogen products, but the 2204-cm^{-1} band grows faster and another band is now detected at 2170 cm^{-1}. The IR spectrum at this stage is illustrated in Figure 5b and UV–vis spectrum in Figure 6a. Irradiation into the UV band ($\lambda = 370$ nm, 180 min) causes growth of Cr(CO)$_3$(dfepe) at the expense of the UV band and the ν(NN) bands above 2200 cm^{-1} (Figures 5c and 6b). The band at 2170 cm^{-1} continues to grow, but the bands of **1** are unchanged. Subsequent irradiation into the visible band of Cr(CO)$_3$(dfepe) ($\lambda > 460$ nm, 720 min) regenerates **1**, the 2226 and 2212 cm^{-1} ν(NN) bands, and the

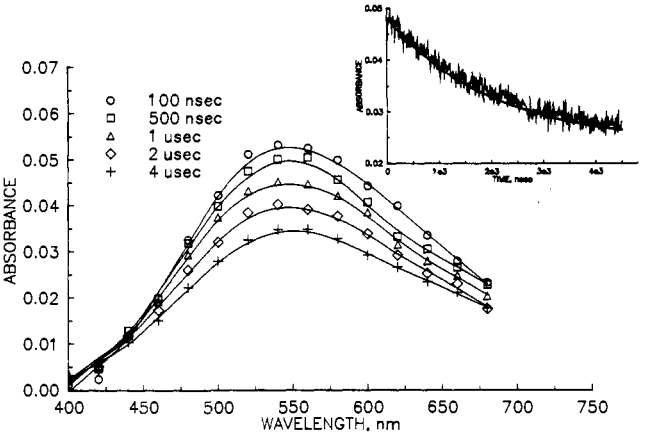

Figure 7. Photolysis ($\lambda = 355$ nm) of **1** (ca. 2 mM) in degassed, dry hexane. The inset shows exponential and a constant using the rates in Table II.

associated UV band. Cr(CO)$_3$(dfepe) and the other two ν(NN) bands are depleted at the same time. However, now the 2212-cm^{-1} feature in the ν(NN) region is formed preferentially (Figures 5d and 6c). A final period of photolysis at 314 nm, which selectively irradiates **1**, generates more Cr(CO)$_3$(dfepe) and restores the intensity ratio of the ν(NN) bands (not illustrated).

This experiment was repeated with a $^{14}N_2/^{15}N_2$/Ar (2.5:2.5:95) matrix in order to determine the stoichiometry of the initial photoproducts. Brief short-wavelength photolysis ($\lambda > 272$ nm, 2 min) was followed by photolysis at $\lambda > 460$ nm (2.5 h) to convert Cr(CO)$_3$(dfepe) to dinitrogen products. The IR difference spectrum from the final stage is shown as a dotted line in Figure 5d. (The subtraction removes almost all the contribution from free CO at 2138 cm^{-1}.) There are two bands at 2213 and 2141 cm^{-1} which display shoulders at 2226 and 2154 cm^{-1}, respectively. These isotope shifts fit to within 3 cm^{-1} of those expected by the reduced mass ratio $(\mu_{14}/\mu_{15})^{1/2}$. The observation that there are no features at intermediate frequencies proves that the 2212- and 2226-cm^{-1} bands arise from monodinitrogen complexes.

Several features of these experiments bear a close resemblance to the reactivity of M(CO)$_6$ (M = Cr, Mo, W) in matrices doped with nitrogen:[7e] (i) the interconversion of products with argon and dinitrogen as sixth ligands; (ii) the position of the UV band; (iii) the frequencies of the ν(NN) modes. For instance, (N_2)Cr(CO)$_5$ exhibits a ν(NN) band at 2240 cm^{-1} and a UV band at 370 nm. However, in the present case four independent ν(NN) modes are observed, two of which are due to monodinitrogen complexes on the basis of their growth after very brief UV photolysis, and again on photolysis at $\lambda > 460$ nm. The presence of one N_2 group is confirmed by the $^{15}N_2$-labeling experiment. These features at 2226 and 2212 cm^{-1} are assigned to *fac*- and *mer*-(N_2)Cr(CO)$_3$(dfepe), respectively.[18] The ν(NN) bands of the initial products and the ν(CO) bands associated with them by their growth patterns are listed in Table I. The assignments of the ν(CO) bands have been verified by calculations using ligand effect constants (see Discussion).

The remaining two ν(NN) bands at 2204 and 2172 cm^{-1} grow on prolonged photolysis and are assigned tentatively to (N_2)$_2$Cr(CO)$_2$(dfepe) isomers (cf. (N_2)$_2$Cr(CO)$_4$),[19] but a dangling monodinitrogen complex of the type (N_2)Cr(CO)$_4$(η^1-dfepe) cannot be excluded for the 2204-cm^{-1} feature.

Nanosecond Transient Absorption. Figure 7 contains spectra from the irradiation of **1** in hexane at times from 50 ns to ca. 4 μs. The maxima (ca. 540 nm) and general spectral features in Figure 7 and from analogous runs in cyclohexane (not shown)

(18) The fac isomer has its N_2 group trans to CO, whereas the mer isomer has N_2 trans to dfepe. Since the ligand effect constants of dfepe are smaller than those for CO, the fac isomer is expected to have its ν(NN) mode to high frequency of the mer isomer.

(19) Turner, J. J.; Simpson, M. B.; Poliakoff, M.; Maier, W. B.; Graham, M. A. *Inorg. Chem.* **1983**, *22*, 911.

(20) Perutz, R. N. Ph.D. Thesis, University of Cambridge, 1974.

Table II. Rate Constants from the Decay of Laser Transients from **1** and **2** in Solution[a]

	from **1**			from **2**		
solvent	k_r, 10^6 s^{-1}	k,[b] 10^6 s^{-1}	k,[c] 10^4 s^{-1}	k_r, 10^6 s^{-1}	k,[b] 10^6 s^{-1}	k,[c] 10^4 s^{-1}
cyclohexane	0.35 (0.08)					
cyclohexane/CO[d]		2.3 (0.6)				
hexane	0.82 (0.03)		*e*	0.76 (0.12)		*f*
hexane/CO[d]		2.6 (0.6)[g]	4.9 (2.3)		2.8 (0.5)	6.5 (0.9)
hexane/Et_3SiH		3.0 (0.3)[h]				
hexane/water		2.9 (0.7)[i]				

[a] Average of first-order rates that were determined at 10–18 different wavelengths and from multiple samples. Standard deviations are given parenthetically. See Scheme II for assignment of rate constants. [b] Assigned to rate in which the intramolecularly coordinated F is replaced. [c] Assigned to rate in which chromium bound solvent is replaced. [d] Solvent is saturated with CO at 1 atm (ref 21). [e] Second-order rate constant: 2.1×10^5 M^{-1} s^{-1}; $\Delta\epsilon^{-1}$ at 560 nm. [f] Second-order rate constant: 2.0×10^5 M^{-1} s^{-1}; $\Delta\epsilon^{-1}$ at 500 nm. [g] For [CO] = ca. 10 mM, second-order rate constant: 2.6×10^8 M^{-1} s^{-1}. [h] Silane is 6.3 mM, second-order rate constant: 4.8×10^8 M^{-1} s^{-1}. [i] Trace amounts of water after drying (ref 23). For $[H_2O] \leq 4$ mM, second-order rate constant $\geq$ ca. 7×10^8 M^{-1} s^{-1}.

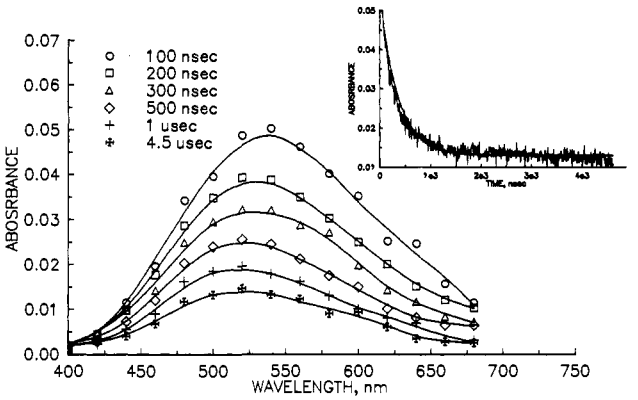

Figure 8. Photolysis (λ = 355 nm) of **1** (ca. 2 mM) in dry hexane saturated with CO. The inset shown the decay at 540 nm fit to a single exponential and a constant using the rates in Table II.

are nearly the same. The inset to Figure 7 is the decay at 540 nm. The decays in hexane and cyclohexane clearly involve at least two processes, a fast one that occurs in the time frame[21] shown and a slower one that is best observed over longer detection intervals (see following section). It is obvious from the longest times in the decay that the transient, which is longer lived and accounts for the slower process, is present in significant quantities relative to the faster-decaying transient.

Figure 8 contains spectra from the irradiation of **1** in CO-saturated[22a] hexane. The inset to Figure 8 shows that the transient decays faster than in the absence of CO in hexane (Figure 7) and cyclohexane and that the concentration of species left at long times is much smaller in magnitude. Note that the peak maximum in Figure 8 shifts toward the blue (shorter wavelength) as time progresses.

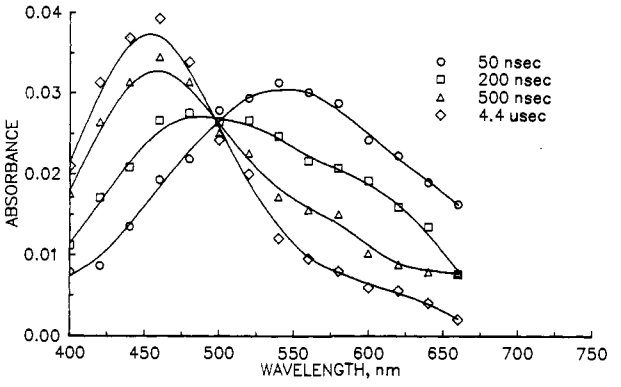

Figure 9. Photolysis (λ = 355 nm) of **1** (ca. 2 mM) with 6 mM Et_3SiH in dry, degassed, dry hexane.

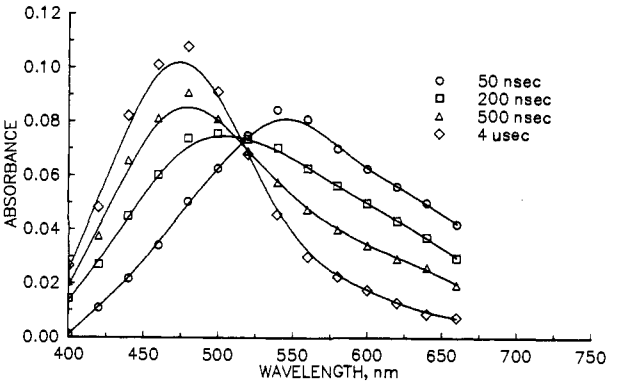

Figure 10. Photolysis (λ = 355 nm) of **1** (ca. 2 mM) in degassed hexane that had not been rigorously dried.

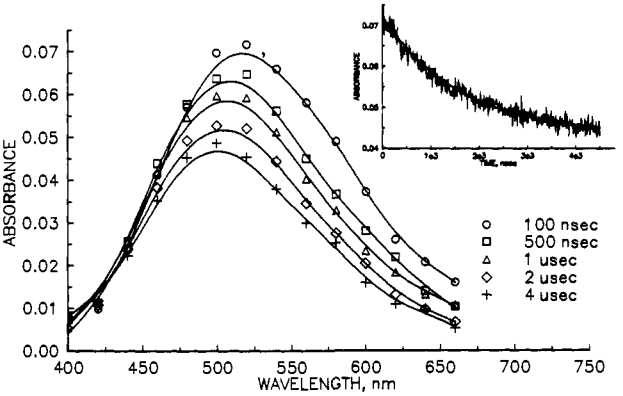

Figure 11. Photolysis (λ = 355 nm) of **2** (ca. 2 mM) in degassed, dry hexane. The inset shows the decay at 520 nm fit to a single exponential and a constant using the rates in Table II.

Spectra from the irradiation of **1** in hexane solutions that contain 6 mM Et_3SiH or a low concentration of water[22b] are shown in Figures 9 and 10, respectively. In the case of silane, the peak

(21) The kinetics from irradiation of **1** in degassed hexane solutions were also measured as a function of the concentration of **1**. Thus, the rate for the fast component from laser flash photolysis of 2 mM **1** in degassed hexane is 8.2×10^5 s^{-1} and is given in Table II. Additional data are as follows (with the standard deviation given parenthetically): 1.4 mM, 7.0 (0.7) $\times 10^5$ s^{-1}; 1.0 mM, 8.7 (0.6) $\times 10^5$ s^{-1}; 0.5 mM, 7.7×10^5 s^{-1}. This suggests that these rates are not a pseudo-first-order process that depends on the concentration of **1** and rules out dimerization between a 16-electron species or a solvent complexed one and the precursor **1**. For an example of such a dimerization see Craven, B. S.; Dixon, A. J.; Kelly, J. M.; Long, C.; Poliakoff, M. *Organometallics* **1987**, *6*, 2600–5.

(22) (a) The solubility of CO when saturated in cyclohexane and heptane is 9.9 and 11.7 mM, respectively: Wilhelm, E.; Battino, R. *Chem. Rev.* **1973**, *73*, 1–9. (b) The exact amount of water was not determined. (Water solubility in hexane or cyclohexane is about 0.01 wt % or ca. 4 mM: Riddick, J. A.; Bunger, W. B. *Techniques of Chemistry*: *Organic Solvents*; Wiley-Interscience: New York, 1970; Vol. II, pp 77–79.) The solvent was dried by distillation from benzophenone ketyl, poured into oven-dried glassware in a glovebox, and subjected to freeze–pump–thaw degassing. (For ultradry conditions 1–3 g of activated molecular sieves was loaded into the glassware, the same procedure was followed, and no peak at 480 nm was observed.) Using the pseudo-first-order rate constant for this reaction (3×10^6 s^{-1}, Table II) and a diffusion-controlled limit of ca. 1×10^{10} M^{-1} s^{-1}, one can estimate the upper limit of water as ca. 3×10^{-4} M. Furthermore, second-order kinetics would be observed if the water concentration approached that of the transient's concentration and that sets the lower limit as ca. 5×10^{-5} M.

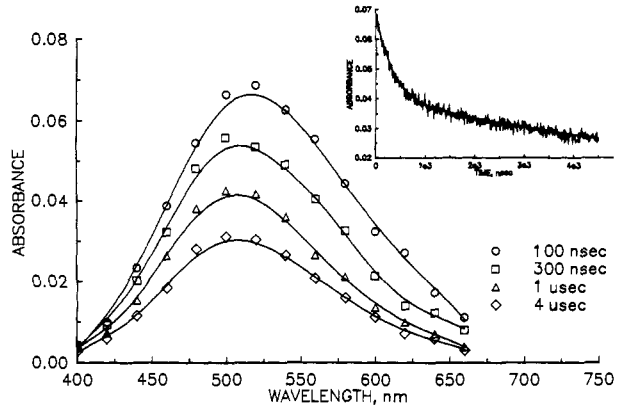

Figure 12. Photolysis (λ = 355 nm) of **2** (ca. 2 mM) in dry hexane saturated with CO. The inset shows the decay at 520 nm fit to a single exponential and a constant using the rates in Table II.

at 540 nm disappears as one at 460 nm appears. Likewise, in Figure 10 the peak at 540 nm gives rise to one at 480 nm. Each demonstrates a well-defined isosbestic point, indicating that the longer wavelength absorbing species (ca. 540–560 nm) give rise to the subsequent short wavelength absorbers (ca. 460–480 nm).

Spectra from the irradiation of $(dfepe)Cr(CO)_5$, **2**, in ultradry hexane and in CO-saturated hexane are shown in Figures 11 and 12, respectively. Both show a maximum at ca. 520 nm that shifts to ca. 500 nm over the measurement time. The decays from both samples are shown as insets to Figures 11 and 12.

The decay rates from the transients observed in Figures 7–12 are compiled in Table II. These data are from fits to a single exponential and a constant. In other words, the second decay is so slow (on the 0–4 μs time scale) that it may accurately be treated as a constant. Alternatively, the data could be fit to two competing exponentials with the following outcome: the first, fast decay gives virtually the same rate constant and preexponential; the second, decays generally fit rates of $(1\text{–}4) \times 10^4\ s^{-1}$, corresponding to half-lives of ca. 20–70 μs. A proper fit to these slow rates should include data over at least five half-lives (i.e., 100–350 μs), and those experiments are considered in the next section.

Microsecond Transient Absorption. The spectra from transients obtained by irradiating the observing samples of **1** and **2** in hexane and CO-saturated hexane on the microsecond time scale are shown in Figures 13 and 14. Complex **1** yields peaks centered at ca. 540 nm in hexane (Figure 13A) or at ca. 520 nm in CO-saturated hexane (Figure 13B). Likewise, **2** gives rise to peaks with maxima at ca. 500 nm in both hexane (Figure 14A) and in CO-saturated hexane (Figure 14B) that differ only in their decay kinetics. The rate constants for the decay of the features in Figures 7 and 8 are included in Table II (columns 3 and 6, respectively). The transients from both **1** and **2** in hexane are best fit to a single, second-order decay, but both yield a fit to a single exponential for the CO-saturated solutions.

Figure 15 contains spectra from **1** and **2**, respectively, in CO-saturated hexane that correspond to the fast and slow components of decay of each. Thus, in Figure 15A the slow component from **1** (rate of decay of $4.9 \times 10^4\ s^{-1}$ in Table II, column 3) corresponds to the transient at later times (ca. 1 μs) in Figure 8. The fast component is simply obtained by subtracting the slow component from the data at earliest times, 100 ns (that is, the spectrum at 100 ns minus the spectrum at 1 μs in Figure 8). The fast component corresponds to a rate of $2.6 \times 10^6\ s^{-1}$ in Table II and has decayed by 96% of its original size in 1 μs. (By contrast, the slow component has only decayed by about 6% at 1 μs, and thus, the determination only requires simple subtraction and not a complex deconvolution.)

The same procedure is used to obtain the fast and slow components to the transient from **2** (Figure 15B). The slow component (rate of $6.5 \times 10^4\ s^{-1}$, Table II) is clearly visible at 1 μs or later in Figure 12. Again, the sum of the fast (rate of $2.8 \times 10^6\ s^{-1}$, Table II) and slow components is equal to the spectrum at 100 ns.

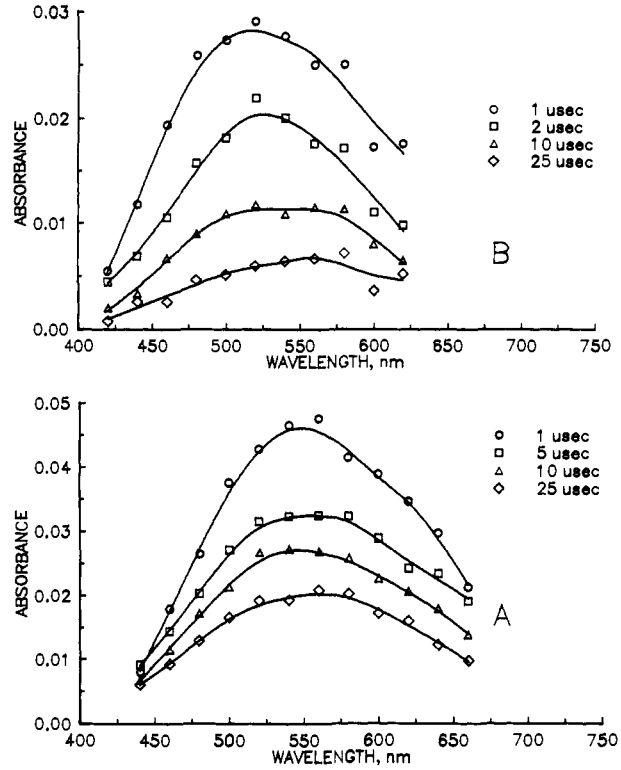

Figure 13. Decay of the slow components from the irradiation (λ = 355 mM) of **1** (ca. 2 mM): A, in dry, degassed hexane; B, in dry hexane saturated with CO.

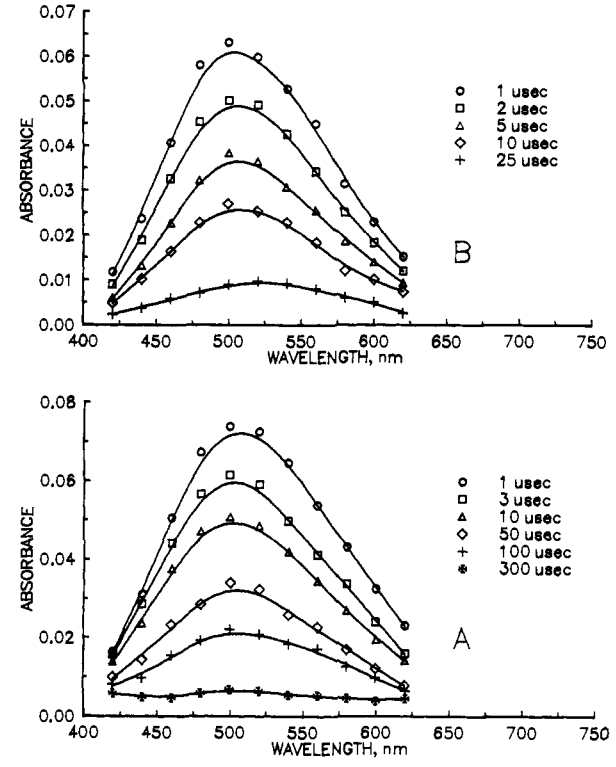

Figure 14. Decay of the slow components from the irradiation (λ = 355 nm) of **2** (ca. 2 mM): A, in dry, degassed hexane; B, in dry hexane saturated with CO.

The spectral features of the data in Figure 15 are quite comparable. Thus, the slow component from **1** has λ_{max} at ca. 520 nm while that from **2** occurs at ca. 500 nm. Likewise, the fast components from **1** and **2** appear at 540 and 560 nm, respectively. The relative intensities are different with the fast component larger than the slow one in Figure 15A while the slow component is larger

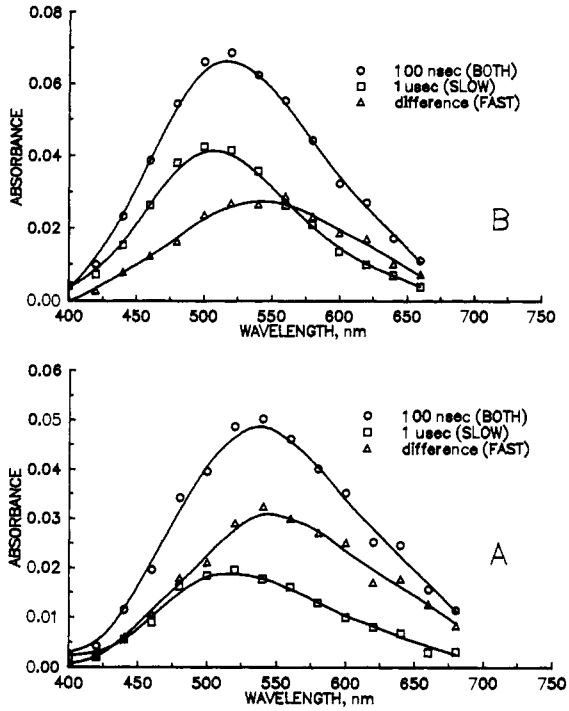

Figure 15. Fast and slow decay components from irradiation (λ = 355 nm) of (A) 1 (ca. 2 mM) in dry hexane saturated with CO and (B) 2 (ca. 2 mM) in dry hexane saturated with CO.

Table III. Relative Ratios of ^{13}C-Labeled Products Formed from Photolysis of 1 under ^{13}CO[a]

P_{CO}, mm	1′-*fac*	1′-*mer*	2′-*cis*	2′-*trans*
115	1.0	0.55	0.35	0.11
295	1.0	0.55	0.49	0.13

[a] Conversions carried out to ca. 5% in cyclohexane solutions.

than the fast one in Figure 15B.

Steady Irradiation and NMR Studies. Irradiation of solutions identical to those used to gather the data for Figures 9 and 10 was conducted in front of a sunlamp. Analysis by infrared or UV–vis spectroscopies confirmed the formation of long-lived products. For example, the solutions turned yellow upon photolysis, and peak maxima at 460 and 480 nm were observed in the presence of silane and water, respectively. No color change was observed in analogous, CO-saturated hexane solutions of 1 that were irradiated with the sunlamp.

The irradiation of 1 in dry cyclohexane solutions under various pressures of ^{13}CO gave us the opportunity to observe the labeling of the starting material and any potential permanent products by ^{13}C NMR spectroscopy. Table III shows the four labeled complexes 1′-*fac*, 1′-*mer*, 2′-*cis*, and 2′-*trans* which are formed. (The position of the ^{13}CO is indicated by the asterisk and fac and mer designations are used to denote the positions of the unlabeled CO ligands.) The data from irradiation at two pressures of ^{13}CO, 113 mm and 295 mm, are given. The relative ratios of products formed are shown and are based on 1′-*fac* as the reference compound.

Discussion

A. Matrix Isolation Experiments. The matrix photochemistry of 1 is summarized in Scheme I. In the rigid matrices, the photochemistry of 1 is dominated by CO loss, leading to two species specifically solvated by the matrix, 4-S-*fac* and 4-S-*mer*, and two species with a fluorine coordinated intramolecularly, 4-F-*fac* and 4-F-*mer* (eq 3). Models show that a fluorine can

$$1 \xrightarrow[\text{Ar or } CH_4]{h\nu,\ -CO} \text{4-S-}fac + \text{4-F-}fac\ (+\ \text{4-S-}mer + \text{4-F-}mer) \qquad (3)$$

coordinate in the sixth position without strain in either mer or fac isomers. Intramolecular interactions between an unsaturated metal center and a C–F bond (eq. M←F–C) have been previously

Scheme I. Matrix Photochemistry of $Cr(CO)_4$(dfepe)

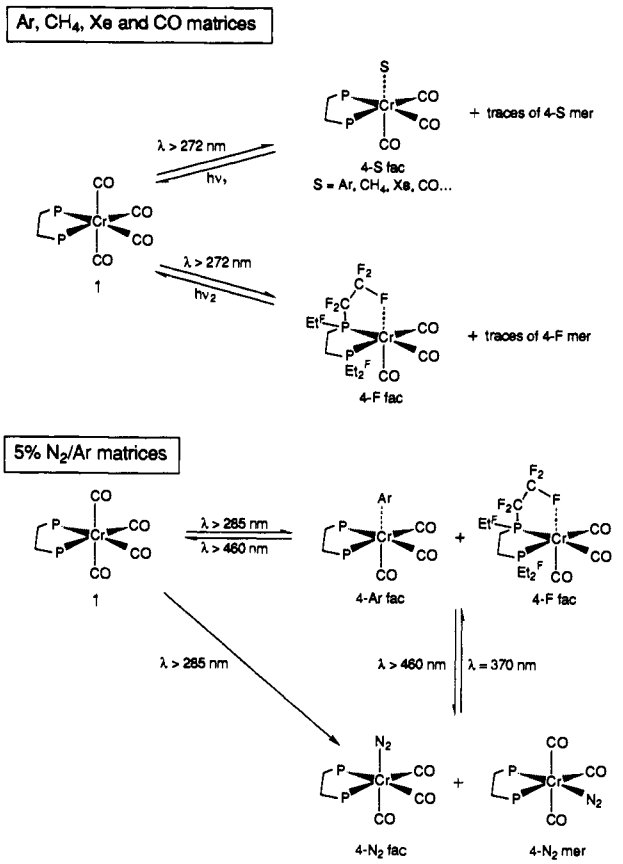

documented for systems involving aryl fluoride bonds.[23] A unique feature of the system reported here is that the C–F bond is part of a perfluoroalkyl group and thus is expected to be a much poorer two-electron donor than simple aryl or alkyl fluorides. The IR data exclude oxidative addition of a C–F bond as has been observed in a few recent examples.[24]

Migration of the bulky $-CH_2-P(C_2F_5)_2$ moiety away from the Cr center after photocleavage of the P–Cr bond is inhibited by the matrix cage. It can be observed in CO matrices, but even then only on prolonged short-wavelength photolysis. In contrast, both Cr–P and Cr–CO bond cleavage are observed on photolysis in solution as is evident from the experiments with steady irradiation (see below). Infrared evidence indicates that the dominant photoproducts in Ar, Xe, and CH_4 matrices are 4-S-*fac* and 4-F-*fac*, with only traces of the mer isomer present. In CO matrices there is less efficient conversion to 4-F-*fac* and the "isocarbonyl" 4-CO-*fac*. In N_2-doped argon matrices, both 4-N_2-*fac* and 4-N_2-*mer* are formed in addition to 4-Ar-*fac* and 4-F-*fac*. The two N_2 complexes are distinguished by their different ν(NN) modes (2226 and 2212 cm^{-1}) and their different growth rates on irradiation into the visible band of 4-Ar-*fac* and 4-F-*fac*.

B. Ligand Effect Constants. Insight into the π-acceptor capability of dfepe can be obtained by calculating its ligand effect constant.[11] At the same time, these calculations provide a check on the consistency of the assignments of the various ν(CO) bands. We use the IR bands of 1, together with the standard ligand effect constants for CO and a first-row d^6 metal, to calculate the two

(23) (a) Kulawiec, R. J.; Crabtree, R. H. *Coord. Chem. Rev.* **1990**, *99*, 89. (b) Thompson, J. S.; Sorrell, T.; Marks, T. J.; Ibers, J. A. *J. Am. Chem. Soc.* **1979**, *101*, 4193. (c) Usow, R.; Fornies, J.; Tomas, M.; Cotton, F. A.; Falvello, L. *J. Am. Chem. Soc.* **1984**, *106*, 2482. (d) Catala, R. M.; Cruz-Garritz, D. M.; Hills, A.; Hughes, D. L.; Richards, R. L.; Sosa, P.; Torrens, H. *J. Chem. Soc., Chem. Commun.* **1987**, 261. (e) Anderson, C. M.; Crespo, M.; Ferguson, G.; Lough, A. J.; Puddephatt, R. J. *Organometallics* **1992**, *11*, 1177.

(24) (a) Richmond, T. A.; Osterberg, C. E.; Arif, A. M. *J. Am. Chem. Soc.* **1987**, *109*, 8091. (b) Jones, W. D.; Partridge, M. A.; Perutz, R. N. *J. Chem. Soc., Chem. Commun.* **1991**, 264.

Table IV. Observed and Calculated ν_{CO} Frequencies (cm^{-1}) Using Refined Ligand Effect Constants ϵ^L_{cis} = 23 and ϵ^L_{trans} = 102 N m^{-1} [a]

	obsd	calcd	error
*1			
a_1	2062	2067	−5
a_1	1998	1993	+5
b_1	1976	1972	+4
b_2	1976	1982	−6
*4-F-*fac*			
a′	2017	2012	+5
a′	1914	1915	−1
a″	1963	1959	+4
*4-F-*mer*			
a′	2038	2037	+1
a′		1964	
a″		1948	
4-N_2-*fac*			
a′	2022	2022	0
a′	1949 sh	1946	+3
a″		1969	
4-N_2-*mer*			
a′	2041	2043	−2
a′		1969	
a″		1958	

[a] Observed bands root mean square error = 3.8 cm^{-1}. Bands observed in methane matrices.

ligand effect constants, ϵ^L_{cis} and ϵ^L_{trans}, of dfepe. The same constants are then used to calculate the force constants and hence the ν(CO) bands of 4-*fac*, 4-*mer*, 4-N_2-*fac*, and 4-N_2-*mer*.

There are three alternative assignments for the ν(CO) bands of **1**. The intense low-frequency band may arise from the overlap either of the b_1 and b_2 modes, or from overlap of b_1 and a_1 modes, or b_2 and a_1 modes. Force constant calculations for **1** in CH_4 employing the first of these assignments give a satisfactory fit to the eight observed frequencies of the unlabeled molecule and the two ^{13}CO-substituted molecules present in natural abundance.[25] The same assignment is the only one to yield reasonable ligand effect constants if the bond angles are kept close to 90°. The resulting ligand effect constants, ϵ^L_{cis} = 25.5 and ϵ^L_{trans} = 95 N m^{-1}, place dfepe between PCl_2Ph and PCl_3 in the ligand effect series and substantially below CO and PF_3. The approximate force constants derived from the ligand effect calculations agree well with the more accurate ones derived from the isotopic data.

We may now use the ligand effect constants to calculate force constants and frequencies for 4-*fac* and 4-*mer* in CH_4. The predicted values for 4-*fac* differ from the experimental values by 5.6 cm^{-1} (root mean square).[26] The predicted values for 4-*mer* are 2038, 1962, and 1951 cm^{-1}, suggesting that the unobserved band of the mer isomer overlaps with the central band of the fac isomer. Similar calculations on $Cr(CO)_2$(dfepe) make it clear that the ν(CO) bands of this species must lie at much lower frequency. If it is assumed that the same ligand effect constants can be employed when dfepe acts as a monodentate dangling ligand as when it is bidentate, we can calculate the positions of the ν(CO) bands of *fac*- and *mer*-$Cr(CO)_4(\eta^1$-dfepe).[26] These frequencies are very far removed from any observed bands, thereby excluding the possibility that the unsaturated dangling molecules are formed in matrices. The assumption that the ligand effect constants may be transferred from the bidentate to the monodentate situation is checked by calculating the frequencies for **2**. If allowance is made for the effect of solvent, agreement is very satisfactory. In addition, we may use the ligand effect constants to predict the ν(CO) frequencies of 4-N_2-*mer* and 4-N_2-*fac*. The high frequency modes, which should be the most sensitive, agree with experiment to within 4 cm^{-1}. Altogether, we have used three observed bands to deduce two adjustable parameters (the ligand effect constants), which have then been used to predict the ν(CO) bands of four further observed species. Finally, we have used the complete set of 11 bands from 5 observed species (using 4-**F**-*fac* and 4-**F**-*mer* as the less perturbed species) to refine the ligand effect constants to values of ϵ^L_{cis} = 23 and ϵ^L_{trans} = 102 N m^{-1} (Table IV). The root mean square error overall in the prediction of 11 bands is 3.8 cm^{-1}, a most satisfactory confirmation of our assignments.

Scheme II

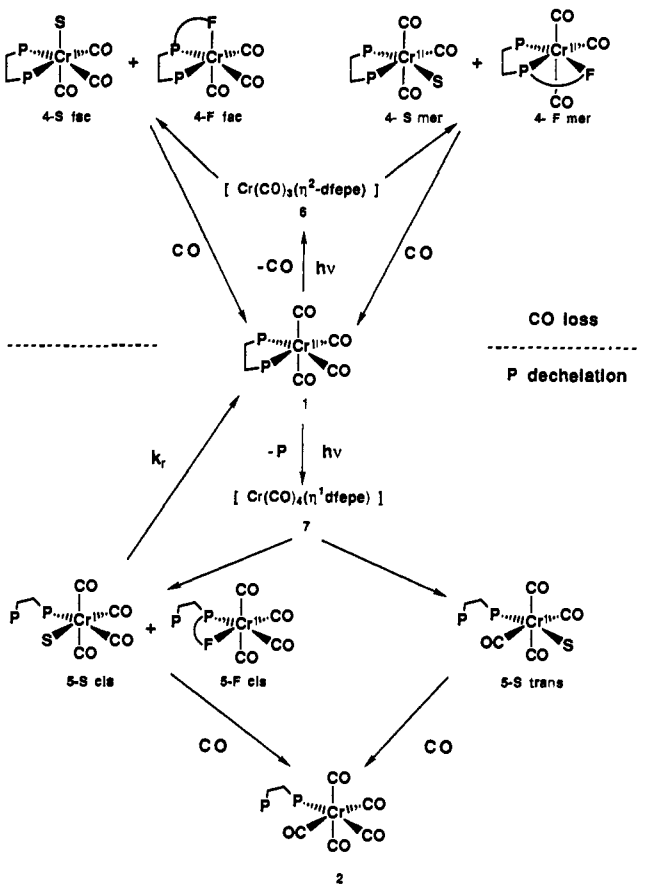

C. Transient Absorption following Photolysis of 1. The results of transient absorption and ^{13}CO labeling experiments from irradiation of **1** in alkane solutions are best rationalized by the reaction sequence shown in Scheme II. The transient absorption data from irradiation of **1** in hexane (Figure 7) and cyclohexane (not shown) give similar results with the initially formed transient (or set of transients) showing λ_{max} centered at 540 nm. An analysis will be presented below which suggests that, in analogy with the matrix experiments, this band is a superposition of a shorter wavelength band due to the presence of alkane complexes 4-**S**-*fac*, 4-**S**-*mer*, 5-**S**-*cis*, and 5-**S**-*trans* (S = hexane or cyclohexane) and a longer wavelength band due to intramolecularly coordinated Cr←F–CF_2– species 4-**F**-*fac*, 4-**F**-*mer*, and 5-**F**-*cis* (intramolecular coordination of F is geometrically prohibited in the 5-*trans* isomer).

Photolysis of **1** in the absence of CO results in a set of transients, one of which exhibits a rapid first-order decay back to **1**. Experiments involving photolysis of **1** under ^{13}C-labeled CO (see below) suggest that intermediates 4-**L**-*fac*, 4-**L**-*mer*, 5-**L**-*cis*, and 5-**S**-*trans* (L = solvent or intramolecularly coordinated F) are all formed in significant quantities. Consideration of the structure of the intermediates suggest that *only* 5-**L**-*cis* can collapse to the starting material via an intramolecular capture process (the

(25) The refined force constants for **1** are (N m^{-1}) k_{ax} 1630, k_{eq} 1612, $k_{ax,eq}$ 25, $k_{eq,eq}$ 35, and $k_{ax,ax}$ 53. The observed and calculated frequencies are (cm^{-1}) as follows (observed values, calculated values, and error, in cm^{-1}): all ^{12}CO 2062, 2061.9, +0.1; 1998, 1997.3, +0.7; 1976, 1975.8, +0.2; 1976, 1975.8, +0.2; ^{13}CO axial 2051, 2050.1, −0.9; 1993 sh, 1993.6, −0.6; (1976), 1975.8, (+0.2); 1945, 1945.4, −0.4; ^{13}CO eq –, 2056.8, –; –, 1991.0, –; (1976), 1975.8, (+0.2); 1942, 1942.6, −0.6. Root mean square error on eight observed bands = 0.40 cm^{-1}.

(26) With the ligand effect constants given in the text and no further refinement, the following ν(CO) frequencies are calculated for CH_4 and 5% Ar/N_2 matrices (ν/cm^{-1}): **1** 2068 (a_1), 1992 (a_1), 1975 (b_2), 1979 (b_1); 4-*fac* 2011 (a′), 1917 (a′), 1956 (a″); 4-mer 2038 (a′), 1962 (a′), 1951 (a″); 4-N_2-*fac* 2021 (a′), 1948 (a′), 1965 (a″); 4-N_2-*mer* 2045 (a′), 1967 (a′), 1961 (a″); $Cr(CO)_4(\eta^1$-dfepe) (C_{4v} isomer) 2067 (a_1), 1956 (e); $Cr(CO)_4(\eta^1$-dfepe) (C_s isomer) 2050 (a′), 1977 (a′), 1956 (a″), 1916 (a′).

Table V. Peak Maxima (nm) from Irradiation of **1**, **2**, and $Cr(CO)_6$ in Indicated Media

	matrix		solution		
medium	**1**[a]	$Cr(CO)_6$	**1**[c]	$Cr(CO)_6$	**2**
neon		624			
argon	545 (S = Ar) 590 (S = F–C)	533			
methane	495 (S = CH_4) 582 (S = F–C)	489	(500)[d]		
CF_4		547			
hexane			510 (slow)[k] 540 (fast)[k]		510 (slow)[k] 560 (fast)[k]
cyclohexane				510	
C_5F_{12}			600[g]	620[f-h]	
Et_3SiH			460		
methanol				460[i]	
water			480	480[j]	

[a] At 12–20 K, this work (see Experimental Section). [b] 12–20 K.[7] [c] In solution in indicated solvent unless otherwise noted, this work. [d] In perfluoroalkane solution. The peak is not well resolved from the one at longer wavelengths. [e] In N_2-saturated hexane. [f] Reference 5. [g] Broad peak that covers much of the visible range 450–750 nm. [h] In perfluoromethylcyclohexane. [i] Reference 2a. [j] Reference 5 and this work. [k] Slow and fast refer to the λ_{max} of the observed and their relative rate of conversion.

rechelation of the bidentate phosphine). Thus, we assign the observed first-order rate constant of 8.2×10^5 s^{-1} in hexane to k_r (see Scheme II and eq 4); λ_{max} does not shift appreciably during

$$\textbf{5-F-}cis\textbf{, 5-S-}cis \xrightarrow{k_r} \textbf{1} \quad (4)$$

this decay process so we have no evidence as to whether **5-S-*cis*** or **5-F-*cis*** or a combination of both are responsible for this decay process. With no externally added CO, the concentration of CO in solution generated by photolysis must be very low (ca (1–3) $\times 10^{-5}$ M) and thus the transients **4-L-*fac***, **4-L-*mer***, and **5-L-*trans*** (which cannot decay by intramolecular processes) all disappear on slower time scales by capture of CO (eqs 5 and 6). (These processes represent the slow component of the reactions in the absence of CO and proceed by second-order rates with the concentration of organometallic intermediate equal to the CO concentration. The second-order rate constants in Table II require an extinction coefficient for the evaluation of their absolute magnitudes.)

$$\textbf{4-F-}fac\textbf{, 4-F-}mer\textbf{, 4-S-}fac\textbf{, 4-S-}mer \xrightarrow{\text{slow, CO}} \textbf{1} \quad (5)$$

$$\textbf{5-F-}trans\textbf{, 5-S-}trans \xrightarrow{\text{slow, CO}} \textbf{2} \quad (6)$$

Upon saturation of the solution with CO, bimolecular capture now essentially dominates the decay processes of the transient intermediates. As noted in the results section, using a combination of nanosecond and microsecond experiments, two transients (or sets of transients) which decay with different rates can be observed. As specified in Table II, the slow component(s) decay with k[CO] $= 4.9 \times 10^4$ s^{-1} while the fast component(s) decay with k[CO] $= 2.6 \times 10^6$ s^{-1}. As illustrated in Figure 15, the slow component exhibits a λ_{max} of ca. 510 nm, while the fast component exhibits λ_{max} ca. 540 nm. Given the very broad nature of these bands and the subtraction procedures used to obtain λ_{max} values, there are substantial uncertainties in these numbers. However, it is clear from Figures 8 and 15 that the faster decaying components absorb at significantly longer wavelengths than the slower decaying components.

In view of the matrix results described above, we believe the most plausible explanation for these observations is that the fast-reacting transients are ones involving intramolecular Cr←F–CF_2– coordination, **4-F-*fac***, **4-F-*mer***, and **5-F-*cis***, while the slowly reacting components are alkane coordinated intermediates (eqs 7–10). Table V summarizes peak maxima of transients generated from **1**, **2**, and $Cr(CO)_6$, in various matrices and solvents. The λ_{max} of ca. 510 nm of the slower transients generated from **1** in hexane compares favorably to the λ_{max} of the **4-CH_4-*fac*** methane complex of 495 nm generated in the methane matrix. Additional support for these assignments is provided by their similarity to values assigned for $Cr(CO)_5(CH_4)$ (matrix, λ_{max} = 489 nm) versus $Cr(CO)_5(C_6H_{12})$ (solution, λ_{max} = 510 nm). The correspondence of the λ_{max} values of **4-F-*fac*** in methane or argon matrices (582 and 590 nm, respectively) with the fast components from **1** in hexane (λ_{max} = 540 nm) is not as good. However, in considering λ_{max}, the extreme breadth of the bands and multiple isomers represent in solution, we regard this assignment as reasonable. Further relevant UV–vis data (Table V) which support these assignments involve observation of a λ_{max} of ca. 500 nm from methane complexes of **4** and **5** in C_5F_{12} solution and the observation of an extremely broad band λ_{max} ca. 620 nm for the transients generated from **1** in C_5F_{12} which must involve the superposition of bands for both intramolecularly coordinated C_5F_{12} and intermolecularly coordinated Cr←F–CF_2– and a multiplicity of isomeric structures.

$$\textbf{4-F-}fac\textbf{, 4-F-}mer \xrightarrow{\text{added CO, fast}} \textbf{1} \quad (7)$$

$$\textbf{5-F-}cis \xrightarrow{\text{added CO, fast}} \textbf{2} \quad (8)$$

$$\textbf{4-S-}fac\textbf{, 4-S-}mer \xrightarrow{\text{added CO, slow}} \textbf{1} \quad (9)$$

$$\textbf{5-S-}cis\textbf{, 5-S-}trans \xrightarrow{\text{added CO, slow}} \textbf{2} \quad (10)$$

The qualitative differences in the rates of reactions of the two sets of transients with CO also support our assignments. Kelly[5e] has shown that $Cr(CO)_5$(alkane) reacts ca. 10^3 times slower with CO than $Cr(CO)_5(C_7F_{14})$. The reactivity differences observed here are only a factor of ca. 50 with the intramolecularly F coordinated species being more reactive than the alkane complexes. It is reasonable to suppose that the intramolecularly coordinated Cr←F–CF_2– bond should be displaced at a slower rate than that of the intermolecularly coordinated fluorocarbon. (Indeed, Kelly argued that the fluorocarbon afforded no stabilization of $Cr(CO)_5$ at all.) This interpretation is comparable to that for the photolysis of $CpW(CO)_3(Et)$ in alkane solvents. Both in alkane glasses and in solution, evidence is found for $CpW(CO)_2(Et)(S)$ and $Cp(CO)_2W(CH_2CH_2–H)$. The latter contains a β-agostic ethyl group.[27]

In the presence of additional, more nucleophilic ligands (i.e., Et_3SiH, water, and N_2), the transients with λ_{max} at ca. 540 nm in hexane disappear and give rise to species formed from displacement of L (L = alkane, F–CF_2–) (see Figures 9 and 10). Because these species appear at shorter wavelengths (and because of the nature of the ligands themselves), we know that these processes are enthalpically driven and substitution gives rise to more stable complexes. In the case of $Cr(CO)_5$)(alkane) the chromium–alkane bond energy has been estimated as to be ca. 10 kcal/mol by Peters[6a] and Burkey.[6d] The lability of the chromium–alkane bond and the rate constants that they measure for the replacement of S (S = alkane) with L (L = ethers, amines,

(27) (a) Kazlauskas, R. J.; Wrighton, M. S. *J. Am. Chem. Soc.* **1982**, *104*, 6005. (b) Yang, G. K.; Peters, K. S.; Vaida, V. *J. Am. Chem. Soc.* **1986**, *108*, 2511. (c) Johnson, F. P. A.; Gordon, C. H.; Hodges, P. M.; Poliakoff, H.; Turner, J. J. *J. Chem. Soc., Dalton Trans* **1991**, 833.

Scheme III

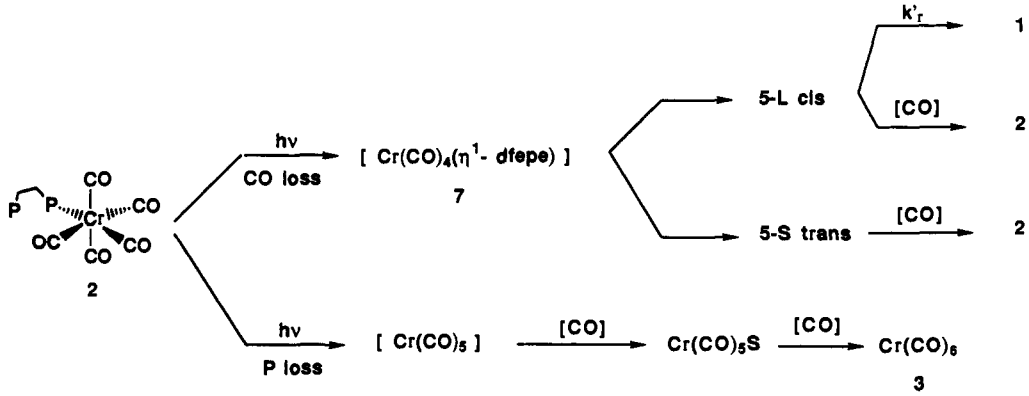

phosphine, etc.) are consistent with the ones that we observe in the present study. For example, in the reactions of the intermediate complex with 6 mM silane (Figure 9), the observed pseudo-first-order rate of 3×10^6 s^{-1} is equivalent to a second-order rate of 3×10^8 M^{-1} s^{-1}.

D. Transient Absorption following Photolysis of 2. We next consider the results of transient absorption spectroscopy of (η^1-dfepe)$Cr(CO)_5$, **2**, in hexane solution. The behavior of **2** is generally similar to that of **1** and supports the above interpretations. The reaction sequence shown in Scheme III will be used in our analysis. As observed for **1**, in the absence of CO one set of transients decays rapidly by a first-order process with $k_r = 7.6 \times 10^5$ s^{-1} (Figure 11, Table II). These transients are proposed to be the **5-L-*cis*** (L = alkane or F). The k_r observed in this case agrees reasonably well with the k_r of 6.1×10^5 s^{-1} measured for the decay of the similar set of transients generated from **1** (the ratio of **5-S-*cis*:5-F-*cis*** generated from **1** vs **2** are likely not the same).

In CO-saturated hexane solutions CO trapping processes predominate. Nanosecond and microsecond transient absorption experiments show, as with **1**, that there are two components to the decay, a fast one with k[CO] = 2.8×10^6 s^{-1} and a slow one with k[CO] = 6.5×10^4 s^{-1}. Figure 15 shows that the slowly decaying component exhibits λ_{max} at shorter wavelengths (ca. 510 nm) relative to the rapdily decaying component (λ_{max} ca. 560 nm). In analogy with **1**, we suggest that the rapidly decaying transient is the intramolecularly coordinated species **5-F-*cis*** as in eq 11 (in

$$\textbf{5-F-}cis \xrightarrow{\text{added CO, fast}} \textbf{2} \qquad (11)$$

contrast to **1**, **4-F-*fac*** and **4-F-*mer*** cannot be formed from **2**). The slowly decaying transients are assigned to the alkane complexes which include **5-S-*cis***, **5-S-*trans***, and $Cr(CO)_5$(S) (S = alkane) (eqs 12 and 13). We have no direct evidence for the formation

$$\textbf{5-S-}cis,\ \textbf{5-S-}trans \xrightarrow{\text{added CO, slow}} \textbf{2} \qquad (12)$$

$$Cr(CO)_5S \xrightarrow{\text{added CO, slow}} Cr(CO)_6 \qquad (13)$$

of $Cr(CO)_5$(S) from **2**; however, judging from the photolability of the Cr–P band in **1**, it is likely formed. It is also of interest to note from Figure 15 that alkane complexes seemed to be formed in relatively larger amounts from **2** than from **1**, a possible consequence of substantial $Cr(CO)_5$(S) formation. The pseudo-first-order rate constant for decay of $Cr(CO)_5$(S) in CO-saturated alkane solution[5] is 3×10^4 s^{-1}, which matches reasonably well our observed slow decay rate.

E. Steady-State Photolysis. Next we consider the ^{13}CO labeling experiments. As noted in Table III, when **1** is photolyzed under ^{13}CO, all four possible labeled products are formed in significant quantities. Scheme IV summarizes the relative ratios of these species at two different pressures of ^{13}CO. As ^{13}CO concentration decreases, **2′-*cis*** decreases. The simplest explanation for this observation is that at the ^{13}CO concentrations used, k_r is competitive with CO trapping of **5-L-*cis***. Thus, as [^{13}CO] decreases, so does the fraction of **2′-*cis*** formed. The transients **4-L-*fac***, **4-L-*mer***, and **5-L-*trans*** have only one reaction mode available and thus **1′-*fac***, **1′-*mer***, and **2′-*trans*** are always formed in similar ratios independent of [^{13}CO].

This explanation is qualitatively consistent with the rate data generated in the transient absorption experiments (Table II). First note that k_r is 6×10^5 s^{-1}. The rate constant for decay of the "fast" transients under 760 mm CO is 2.6×10^6 s^{-1}, so this rate at 115 and 295 mm CO can be estimated as 3.9×10^5 and 1.0×10^6 s^{-1}, respectively. These two rates are clearly competitive with the rate of return (k_r) and thus in accord with an increase in **2′-*cis*** with increasing ^{13}CO pressure. A quantitative analysis is precluded by the fact that we are not able to dissect k_r into the return rate constant for **5-F-*cis*** and **5-S-*cis*** nor can we determine precisely k_{3F}[CO] and k_{3S}[CO].

The mechanistic scheme developed above illustrates a significant point regarding the structure and dynamics of the initially generated 16-electron intermediates **6** and **7**. Earlier work has established that in the case of $Cr(CO)_5$ capture by solvent (e.g., alkanes) occurs on the picosecond time scale.[2] When photodissociation of the Cr–P bond of **1** occurs, the initial geometry of **7** must be square pyramidal (SP) with an open cis coordination site. Given that both **5-L-*cis*** and **5-L-*trans*** are formed from capture of **7** on a picosecond time scale, the initially formed SP species must either equilibrate with a SP species having the empty coordination site trans to phosphine or collapse to a trigonal-bipyramidal structure which can be captured to give either **5-L-*cis*** or **5-L-*trans***. By analogy, the dynamic behavior of **6** is no doubt similar to that of **7**. Thus, we cannot draw any conclusions concerning the relative photolabilities of the two nonequivalent CO ligands in **1** based on the observed ratios of **4-L-*fac*** and **4-L-*mer*** as judged from the ^{13}CO trapping experiments. In the matrix experiments, however, it is apparent that initial formation of **4-L-*fac*** is preferred over formation of the mer isomers, indicating an increased photolability of the CO ligand cis to both phosphorus ligands.

The ^{13}CO labeling results reveal substantial differences in initial photoproducts of **1** in the matrix experiments where **4-L-*fac*** is the dominant product and the solution experiments where all four isomers **4-L-*fac***, **4-L-*mer***, **5-L-*cis***, and **5-L-*trans*** are formed in significant quantities. These differences can be reconciled as follows. First, although the Cr–P bond may undergo photodissociation in matrices, the migration of the bulky $-CH_2-P(C_2F_5)_2$ group away from the metal center is inhibited by the matrix, and thus, no products of the type η^1-(dfepe)$Cr(CO)_4$L are observed. Second, matrix experiments show that the cis CO ligands are much more photolabile than the trans CO ligands. Assuming similar lability differences in solution, it is reasonable to suppose that the **4-L-*mer*** products are formed primarily by photodissociation of cis CO ligands followed by rearrangement of the 16-electron intermediate and capture to give **4-L-*mer*** products. This explanation is consistent with formation of **5-L-*trans*** from **1**.

The observation that the initially generated square-pyramidal, 16-electron d^6 L_5M moiety undergoes isomerization in solution before solvent capture has precedent. Dobson et al.[28] have noted

Scheme IV

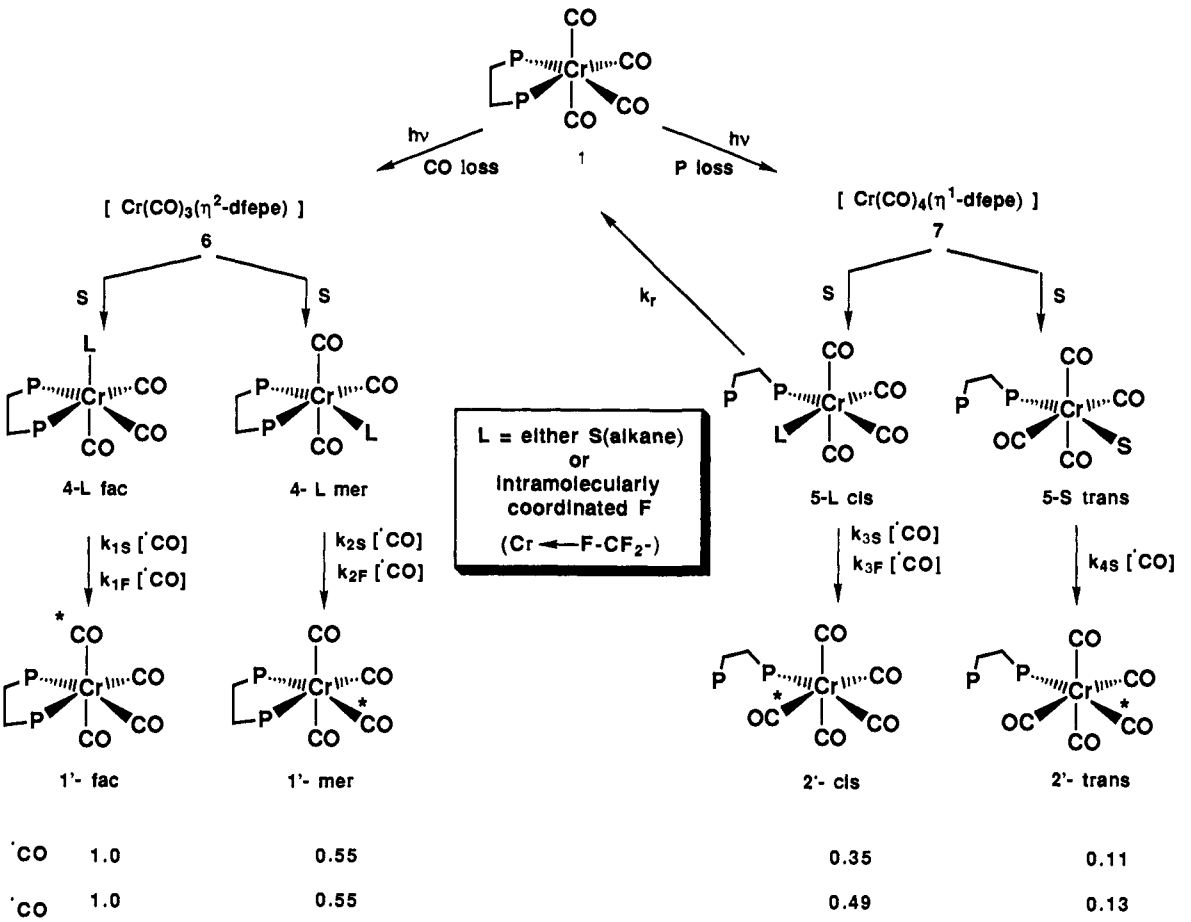

115 mm CO	1.0	0.55	0.35	0.11
295 mm CO	1.0	0.55	0.49	0.13

that photolysis of the chelate [1-(diethylamino)-2-(diphenylphosphino)ethane]$Mo(CO)_4$ (η^2-(NP)$Mo(CO)_4$) in chlorobenzene led to Mo–N bond fission and formation of *both cis-* and *trans*-η^1-(NP)$Mo(CO)_4$(solvent). For the cis solvate, ring closure back to η^2-(NP)$Mo(CO)_4$ and capture by $P(C_6H_5)_3$ or phosphites are competitive. A second example comes from the work of Dobson, Turner, and Paliakoff[29] in which photolysis of *cis*-$W(CO)_4$(piperidine)(L) (L = $P(C_6H_5)_3$, $P(OR)_3$) led to loss of piperidine and formation of both *cis-* and *trans*-$(CO)_4W$(solvent)(L).

Given the similarity in the electronic structure between **1** and $Cr(CO)_6$ and between their respective unsaturated species, **1** is a likely candidate for time-resolved IR and for the picosecond (and faster) spectroscopy experiments, where one might hope to identify more definitively the structural dynamics involved in the skeletal rearrangement of the naked species, **6**. The reduced symmetry of **1** and its photoproducts may provide additional means of following dynamic rearrangements.

Conclusions

Photolytic studies of (dfepe)$Cr(CO)_4$, an analogue of $Cr(CO)_6$ in which two CO ligands have been replaced by the strong π-acceptor bidentate ligand $(C_2F_5)_2PCH_2CH_2P(C_2F_5)_2$, have been conducted in rigid matrices at 12 K (Ar, CH_4, N_2, CO) and 30 K (Xe) and in alkane and perfluoroalkane solutions. In Ar, CH_4, and Xe matrices a combination of IR and UV–vis spectroscopic data demonstrate photodissociation of the cis carbonyl ligand to generate *fac*-(dfepe)$Cr(CO)_3$L, where L is either the matrix host or an intramolecularly coordinated F atom donated by one of the pendant CF_3CF_2– groups of the dfepe ligand. Only traces of the mer isomer are observed. In nitrogen matrices there is evidence for formation of both fac- and mer-(dfepe)$Cr(CO)_3N_2$. There is no evidence for initial formation of products resulting from photodissociation of the P–Cr bond; however, with prolonged irradiation in a CO matrix some evidence for (η^1-dfepe)$Cr(CO)_5$ exists. Carbonyl stretching frequencies of the matrix-isolated photoproducts were measured and bonding force constants and ligand effect constants were calculated.

In solution both the Cr–CO and Cr–P bonds are photolabile. Results of nanosecond and microsecond transient absorption spectroscopic experiments in hexane and cyclohexane solvents indicate formation of alkane complexes of the type (η^2-dfepe)$Cr(CO)_3$(alkane) and (η^1-dfepe)$Cr(CO)_4$(alkane), as well as formation of intramolecularly F-coordinated species $Cr(CO)_4$-(η^1-dfepe) and $Cr(CO)_3$(η^2-dfepe). Rates of reaction of these species in alkane solvents with and without added trapping ligands (CO, water, triethylsilane) have been measured. The F-coordinated species react with CO approximately 50 times faster than the alkane complexes. In transient absorption experiments using (η^1-dfepe)$Cr(CO)_5$, **2**, similar results have been obtained which support the interpretation of the behavior of **1**.

Products from ^{13}CO trapping of the transients generated in cyclohexane show that all four possible isomers, *fac-* and *mer*-(η^2-dfepe)$Cr(CO)_3$*CO and *cis-* and *trans*-(η^1-dfepe)Cr-$(CO)_4$*CO, are formed in significant quantities. Experiments carried out at different ^{13}CO pressures show that ^{13}CO trapping of *cis*-(η^1-dfepe)$Cr(CO)_4$(L) is competitive with ring closure back to **1** ($k = 6 \times 10^5$ s^{-1}). Production of *trans*-(η^1-dfepe)Cr-$(CO)_4$(alkane) from **1** implies that the initially formed 16-electron square-pyramidal (η^1-dfepe)$Cr(CO)_4$ either equilibrates with the other SP isomer or rearranges to a trigonal-bipyramidal structure on a (sub)picosecond time scale prior to solvent trapping.

In the present study, stable alkane complexes (e.g., *cis-* and *trans*-(η^2-dfepe)$Cr(CO)_3$(alkane)) could not be isolated or observed

(28) Dobson, G. R.; Bernal, I.; Reisner, G. M.; Dobson, C. B.; Mansour, S. E. *J. Am. Chem. Soc.* **1985**, *107*, 525.

(29) Dobson, G. R.; Hodges, P. M.; Healy, M. A.; Poliakoff, M.; Turner, J. T.; Firth, S.; Asali, K. J. *J. Am. Chem. Soc.* **1987**, *109*, 4218.

by NMR spectroscopy due to rapid back reaction with the CO produced in the photolysis. Studies on Fe(0) complexes of dfepe suggest that the bulky bidentate ligand is able to prevent clustering reactions of unsaturated species.[30] Thus, given the substantial Cr-alkane binding energy in (dfepe)$Cr(CO)_3$(alkane), it seems plausible that this alkane complex could be observed in NMR experiments if it could be generated in the absence of CO or other ligands capable of displacing the alkane. Experiments along these lines are planned.

(30) Brookhart, M.; Chandler, W. A.; Pfister, A. C.; Santini, C. C.; White, P. S. *Organometallics* **1992**, *11*, 1263.

Acknowledgment. We acknowledge the Gas Research Institute (Contract No. 5076-260-1596) for financial support of this work. C.C.S. acknowledges CNRS for financial support. We thank T. J. Meyer for the use of laser transient instrumentation. R.N.P. and C.H. acknowledge the support of SERC, The Royal Society, British Gas, and the European Commission. J.A.T. acknowledges the support of the Leverhulme Trust.

Electron Transfer in $Fe^{II}Fe^{III}$ Model Complexes of Iron-Oxo Proteins

Mark S. Mashuta,[†] Robert J. Webb,[‡] James K. McCusker,[‡] Edward A. Schmitt,[‡] Kenneth J. Oberhausen,[†] John F. Richardson,[†] Robert M. Buchanan,*[,†] and David N. Hendrickson*[,‡]

Contribution from the Department of Chemistry, University of Louisville, Louisville, Kentucky 40292, and the Department of Chemistry-0506, University of California at San Diego, La Jolla, California 92093-0506. *Received February 7, 1991*

Abstract: The nature of valence trapping is studied for a series of six μ-phenoxo-bis(μ-carboxylate)-bridged $Fe^{II}Fe^{III}$ complexes. The septadentate ligand $bimp^-$ binds the two metal ions and provides a phenoxide bridge as well as four imidazole moieties. The X-ray structure of $[Fe^{II}Fe^{III}(bimp)(\mu\text{-}O_2CPh)_2](BPh_4)_2\cdot{}^3/_2CH_3CN$ at 295 K is reported. This mixed-valence complex crystallizes in the $P\bar{1}$ space group with unit cell parameters of a = 15.995 (4) Å, b = 23.475 (4) Å, c = 11.464 (4) Å, α = 97.57 (1)°, β = 101.74 (1)°, γ = 85.22 (1)°, and Z = 2. A total of 11334 unique data with $I > 3\sigma(I)$ were refined to values of R = 0.045 and R_w = 0.051. The structure shows distinct octahedral (N_3O_3) high-spin Fe^{III} and Fe^{II} ions, with an Fe···Fe distance of 3.440 Å. The phenoxide Fe^{II}–O–Fe^{III} bridging angle is 115.17 (8)°. The BPh_4^- ions are not symmetrically distributed about the $Fe^{II}Fe^{III}$ cation; they are closer to the Fe^{II} ion than the Fe^{III} ion. Sharp ^1H NMR signals spanning a chemical shift range of ~350 ppm are seen for CD_3CN solutions of the $Fe^{II}Fe^{III}$ complexes. Relative to the ^1H NMR timescale these mixed-valence complexes are rapidly transferring electrons in solution. This is due to either rapid *intra*molecular electron transfer or rapid electron transfer between binuclear complexes. A weak intervalence transfer (IT) electronic absorption band is seen at ~1300 nm (ϵ = ~200 M^{-1} cm^{-1}) for all six $Fe^{II}Fe^{III}$ complexes in solution. Two quasireversible one-electron waves corresponding to the $Fe^{II}Fe^{II}/Fe^{II}Fe^{III}$ and $Fe^{II}Fe^{III}/Fe^{III}Fe^{III}$ couples are seen for each complex by cyclic voltammetry. The two waves observed for the $Fe^{II}Fe^{III}$(bimp) complexes occur at potentials 100–300 mV more negative than those reported for the analogous polypyridyl and benzimidazole complexes. Variable-temperature (5–300 K) magnetic susceptibility data are presented for two of the $Fe^{II}Fe^{III}$ complexes. These data were least-squares fit in a matrix diagonalization approach including the effects of Heisenberg magnetic exchange ($\hat{H} = -2J\hat{S}_1\cdot\hat{S}_2$), isotropic Zeeman and axial single-ion zero-field ($D\hat{S}_{z^2} - {}^1/_3S(S + 1)$] for both Fe^{II} and Fe^{III} interactions. Fitting of the data for one sample of $[Fe^{II}Fe^{III}(bimp)(\mu\text{-}O_2CCH_3)_2](ClO_4)_2\cdot 2H_2O$, for example, gave parameters of J = −3.4 cm^{-1}, $D(Fe^{II})$ = 0.63 cm^{-1}, and $g(Fe^{II})$ = 1.86. There is a $S = {}^1/_2$ ground state; however, the $S = {}^3/_2, {}^5/_2, {}^7/_2$, and ${}^9/_2$ excited states are near to the ground state. ^{57}Fe Mössbauer spectroscopy was used to thoroughly examine the temperature dependence of valence detrapping seen for the $Fe^{II}Fe^{III}$(bimp) complexes. It is shown that several of these complexes exhibit valence detrapping (onset of rapid electron transfer relative to the ^{57}Fe Mössbauer timescale) as the temperature is increased. Furthermore, there is a dependence on which anions and solvate molecules are present. Electron paramagnetic resonance (EPR) signals which are similar to those reported for the $Fe^{II}Fe^{III}$ forms of iron–oxo proteins such as hemerythrin, ribonucleotide reductase, purple acid phosphatase, and methane monooxygenase are found for liquid-helium-temperature CH_3CN solutions of the $Fe^{II}Fe^{III}$(bimp) complexes. The EPR signals are sensitive to sample conditions (frozen solution, polycrystals, etc.). The importance of the data observed for the $Fe^{II}Fe^{III}$(bimp) complexes in understanding observations on the iron–oxo proteins is discussed.

Introduction

Dinuclear oxo-bridged iron centers are known or believed to occur in the metalloproteins hemerythrin,[1-13] ribonucleotide reductase,[14-19] purple acid phosphatase,[20-24] uteroferrin,[20,25-33] and methane monooxygenase.[34-37] Hemerythrin (Hr), which is considered the prototype for this class of metalloproteins, has been shown crystallographically[5,8-10] to contain a dinuclear (μ-oxo-bis(μ-carboxylato)) iron core structure in its met form. Three histidines complete the octahedral coordination of one ferric ion while two histidines and an azide are coordinated to the second iron site in N_3-met-Hr. Ribonucleotide reductase,[14] on the other hand, has a μ-oxo-μ-carboxylato bridged Fe_2 active site and

[†] University of Louisville.
[‡] University of California at San Diego.

(1) Wilkins, P. C.; Wilkins, R. G. *Coord. Chem. Rev.* **1987**, *79*, 195-214.
(2) Klotz, I. M.; Kurtz, D. M., Jr. *Acc. Chem. Res.* **1984**, *17*, 16-22.
(3) (a) Lippard, S. J. *Angew. Chem., Int. Ed. Engl.* **1988**, *27*, 344-361. (b) Que, L., Jr. *ACS Symp. Ser.* **1988**, *No. 372*, 152-178. (c) Vincent, J. B.; Olivier-Lilley, G. L.; Averill, B. A. *Chem. Rev.* **1990**, *90*, 1447-1467.
(4) Wilkins, R. G.; Harrington, P. C. *Adv. Inorg. Biochem.* **1988**, *5*, 51-85.
(5) Klotz, I. M.; Klippenstein, G. L.; Hendrickson, W. A. *Science (Washington, D.C.)* **1976**, *192*, 335-344.
(6) Sanders-Loehr, J. In *Frontiers in Bioinorganic Chemistry*; Xavier, A. V., Ed.; VCH: Weinheim, 1986; pp 574-582.
(7) Sanders-Loehr, J.; Loehr, T. M. *Adv. Inorg. Biochem.* **1979**, *1*, 235-252.

0002-7863/92/1514-3815$03.00/0